High-throughput isotherm determination and thermodynamic modeling of protein adsorption on mixed mode adsorbents

Beckley K. Nfor, Marc Noverraz, Sreekanth Chilamkurthi, Peter D.E.M. Verhaert, Luuk A.M. van der Wielen, Marcel Ottens*

Department of Biotechnology, Delft University of Technology, Julianalaan 67, 2628 BC, Delft, The Netherlands

ABSTRACT

The thermodynamic modeling of protein adsorption on mixed-mode adsorbents functionalized with ligands carrying both hydrophobic and electrostatic groups was undertaken. The developed mixed mode isotherm was fitted with protein adsorption data obtained for five different proteins on four different mixed mode adsorbents by 96-well microtitre plate high throughput batch experiments on a robotic workstation. The developed mixed mode isotherm was capable of describing the adsorption isotherms of all five proteins (having widely different molecular masses and iso-electric points) on the four mixed mode adsorbents and over a wide range of salt concentrations and solution pH, and provided a unique set of physically meaningful parameters for each resin–protein–pH combination. The model could capture the typically observed minimum in mixed mode protein adsorption and predict the precise salt concentration at which this minimum occurs. The possibility of predicting the salt concentration at which minimum protein binding occurs presents new opportunities for designing better elution strategies in mixed mode protein chromatography. Salt–protein interactions were shown to have important consequences on mixed mode protein adsorption when they occur. Finally, the mixed mode isotherm also gave very good fit with literature data of BSA adsorption on a different mixed mode adsorbent not examined in this study. Hence, the mixed mode isotherm formalism presented in this study can be used with any mixed mode adsorbent having the hydrophobic and electrostatic functional groups. It also provides the basis for detailed modeling and optimization of mixed mode chromatographic separation of proteins.

© 2010 Elsevier B.V. All rights reserved.

1. Introduction

The excellent selectivity properties and relatively mild conditions in liquid chromatography have made it indispensable in the downstream process development of therapeutic proteins for which very high purity of the active product is paramount and the time-to-market short [1,2]. While the vast majority of chromatographic media used for protein purification today are designed to operate in single interaction mode such as size exclusion, electrostatic interaction, hydrophobic interaction and bioaffinity interaction [3], multimodal or mixed mode chromatographic media, on the other hand, are intentionally functionalized with ligands capable of two or more orthogonal modes of interactions to effect the separation.

Most mixed mode resins used for protein applications are functionalized with ligands exhibiting both hydrophobic and electrostatic properties [4–6]. The electrostatic part can effect

adsorption at low to moderate conductivities while the hydrophobic part does so at moderate to high conductivities, thereby extending the range of selectivity of the adsorbent [5]. Desorption is induced by charge repulsion, accomplished by changing the pH of the mobile phase across the pI of the protein [7,8] or across the pK_a of the ligand in the case of hydrophobic charge induction chromatography (HCIC) [9]. The main advantage of mixed mode resins is the wider range of selectivity that may be achieved in a single column compared to conventional ion exchange chromatography (IEX) or hydrophobic interaction chromatography (HIC) [10]. Hence, one mixed mode chromatographic column can potentially replace two orthogonal chromatographic steps in a protein purification process, with clear cost benefits. Another advantage is the potential for direct protein capture from unadjusted moderate to high conductivity feeds, thereby minimizing the need for feed pretreatment [11,12]. Mixed mode chromatography also finds applications in proteomics studies where it has been used for pre-fractionation of protein mixtures for further analysis by mass spectrometry [13].

Gao et al. [4,14,15] investigated mixed mode adsorbents functionalized with benzylamine ligand for expanded bed applications,

* Corresponding author. Tel.: +31 0152782151; fax: +31 0152782355.
E-mail address: m.ottens@tudelft.nl (M. Ottens).

using bovine serum albumin (BSA) as a model protein. The adsorbents showed salt-tolerant and pH-dependent protein binding and effective protein desorption by charge repulsion [14,15]. BSA binding capacities on the mixed mode adsorbents were higher than on traditional IEX adsorbents [14]. Using pre-packed mini-columns, Brochier et al. [7] screened three different mixed mode chromatography adsorbents and found each of them to display a higher binding capacity and unique selectivity for protein separation under physiological conditions compared to conventional HIC.

Inspite of the vast potentials of mixed mode adsorbents for industrial applications, detailed theoretical treatment of protein interactions by mixed mode mechanisms is still largely sparse. Isotherm formalisms developed for IEX and HIC have not only enabled better characterization of protein binding on these modes of chromatography, but have also reduced the amount of experimentation needed for process development [16–22]. Likewise, a better understanding of protein adsorption on mixed mode adsorbents is an important requirement for more optimal exploitation of this mode of chromatography for industrial scale purification. This will also pave the way for detailed model-based simulation and optimization of protein purification by mixed mode chromatography.

Available isotherms for mixed mode protein adsorption are mostly empirical. Melander et al. [23] presented a simplified three-parameter model describing the effect of salt on the retention behavior of proteins in mixed mode chromatography based on electrostatic and hydrophobic interactions. Their simplified theoretical treatment enabled the characterization of various stationary phases and proteins by analyzing the protein retention data [23]. Chang et al. [24] and Gao et al. [8] used the typical two-parameter Langmuir isotherm to correlate isotherm data obtained for BSA on STREAMLINE Direct HST mixed mode adsorbent designed for expanded bed applications. Although the traditional Langmuir isotherm provides useful information on the maximum binding capacity and dissociation constant, it does not incorporate the influence of the adsorbent and the mobile phase condition on protein interaction, and must therefore be applied to each condition separately. Ghose et al. [9] proposed an exponentially modified nonlinear Langmuir isotherm for describing both the pH and salt concentration dependence of protein adsorption in HCIC. A similarly modified Langmuir isotherm was used by Gao et al. to study the adsorption behavior of BSA on their mixed mode adsorbents [14]. In all these cases, the modified Langmuir isotherm could be successfully fitted to protein adsorption isotherm data obtained over a range of pH and mobile phase salt concentrations, with only a single set of parameters. However, the parameters in the modified Langmuir isotherm were only empirical, with no physical meaning. Moreover, most of these investigations have mainly focused on BSA as a model protein [8,14,15,24,25]. More mechanistic models for describing mixed mode protein adsorption need to be developed and applied to model proteins of widely different properties.

This study focuses on the thermodynamic modeling of protein adsorption on mixed-mode adsorbents functionalized with ligands carrying both hydrophobic and electrostatic groups. The model derivation follows the hermeneutics of the generalized thermodynamic framework used by Mollerup for IEX and HIC [17,18]. The isotherm is fitted with protein adsorption data obtained for five different proteins on four different mixed mode resins by 96-well microtitre plate high throughput (HT) batch experiments on a robotic workstation. HT batch experiments offer considerable savings in time and material compared to traditional column experiments [26,27]. Additionally, the model was challenged by fitting isotherm data obtained by Gao et al. [14] for their mixed mode adsorbent functionalized with benzylamine ligands. The presented mixed mode adsorption isotherm formalism provides a unique set of physically meaningful parameters capable of describing the adsorption of different proteins over a wide range of operating conditions, which would otherwise require an enormous amount of experimentation.

2. Theory

2.1. Mollerup's thermodynamic framework

Mollerup developed a generalized thermodynamic framework for protein adsorption in IEX and HIC and an approach for estimating the unknown model parameters [17,18,20,22]. The general form of the isotherm for a multicomponent system is given by:

$$\frac{q_{p,i}}{c_{p,i}} = A_i \left(1 - \sum_{j=1}^{m} \frac{q_{p,j}}{q_{p,j}^{\max}} \right)^{v_i} \tag{1}$$

where v is the stoichiometric coefficient, c_p is the liquid phase protein concentration, q_p and $q_p^{\max}$ are the adsorbed phase protein concentration and the maximum binding capacity, respectively, subscripts i and j represent species in a multi-component system of m proteins, and A_i is the initial slope of the isotherm or the partition coefficient. The term $1 - \sum_{j=1}^{m}(q_{p,j}/q_{p,j}^{\max})$ gives the fraction of free ligands. A_i is dependent on the adsorption mechanism and is determined from isocratic retention data measured under linear conditions [20].

In hydrophobic interaction chromatography, the initial slope of the isotherm is given by:

$$A_i = \left(\frac{\Lambda}{c} \right)^{v_i} \tilde{K}_i \tilde{\gamma}_i = \left(\frac{\Lambda}{c} \right)^{v_i} \exp \left(\frac{\Delta \tilde{G}_i^\circ}{RT} \right) \tilde{\gamma}_i = A_{0,i} \tilde{\gamma}_i \tag{2}$$

where Λ is the ligand density, $\tilde{K}_i$ is the thermodynamic equilibrium constant, c is the molar concentration of solution in the pore volume, $\Delta \tilde{G}_i^\circ$ is the standard Gibbs energy of association, R is the molar gas constant, T is the temperature, $\tilde{\gamma}_i = \gamma_i / \gamma^{\infty,w}$ is the asymmetric activity coefficient of the solute, γ_i is its activity coefficient in solution, and $\gamma^{\infty,w}$ is its activity coefficient in pure water.

In ion exchange chromatography, the initial slope is given by:

$$A_i = \left(\frac{\Lambda}{c_s z_s} \right)^{v_i} K_i = \left(\frac{\Lambda}{c_s z_s} \right)^{v_i} \exp \left(-\frac{\Delta G_i^\circ}{RT} + v_i \frac{\Delta G_s^\circ}{RT} \right) \tag{3}$$

where c_s is the salt concentration, z_s is the charge on the salt counter-ion, $v_i = z_{p,i}/z_s$ is the stoichiometric coefficient, $z_{p,i}$ is the binding charge of the protein. For monovalent counter-ions ($z_s = 1$), the model is equivalent to the steric mass action model for protein adsorption in IEX [16], with the maximum binding capacity, $q^{\max} = \Lambda/(z_p + \sigma)$, where Λ is the ionic capacity of the resin and σ is the steric hindrance factor.

2.2. HIC–IEX mixed mode isotherm

In the proposed thermodynamic treatment of mixed mode protein adsorption, the following mixed mode interaction stoichiometry is assumed,

$$P + v SL + n L \Leftrightarrow PL_n + v S \tag{4}$$

in which a protein molecule P can interact with n hydrophobic ligands and simultaneously exchange with v salt counter-ions on the resin surface to form the protein–ligand complex PL_n. The thermodynamic equilibrium constant can be written in terms of the activities of the species or the standard Gibbs energy change of association as:

$$K_{eq} = \frac{a_{PL_n}}{a_p} \left(\frac{a_s}{a_{SL}} \right)^v \left(\frac{1}{a_L} \right)^n \equiv \exp \left(-\frac{\Delta G_p^\circ}{RT} + v \frac{\Delta G_s^\circ}{RT} \right) \tag{5}$$

Eq. (5) can be re-written in terms of the activity coefficients of the species as:

$$K_{eq} = \left(\frac{q_p \gamma_{PL_n}}{c_p \gamma_p} \right) \left(\frac{c_s \gamma_s}{q_s \gamma_{SL}} \right)^v \left(\frac{c}{c_L \gamma_L} \right)^n \tag{6}$$

By assuming that the activity coefficient of all other species but the protein solute is unity (i.e. $\gamma_{PL_n} = \gamma_s = \gamma_L = 1$), the thermodynamic equilibrium constant can be approximated to:

$$K_{eq} \cong \left(\frac{q_p}{c_p} \right) \left(\frac{c_s}{q_s} \right)^v \left(\frac{c}{c_L} \right)^n \left(\frac{1}{\gamma_p} \right) \tag{7}$$

where q_p and q_s are the adsorbed phase concentrations of the protein and salt, respectively, c_p and c_s are the liquid phase concentrations of protein and salt, respectively, c_L is the concentration of free ligands, c is the molarity of the solution in the pore volume, γ_p is the activity coefficient of the protein in solution, n is the stoichiometric coefficient of the ligand and $v = z_p/z_s$ is the stoichiometric coefficient of the salt counter-ion, where z_p is the effective binding charge of the protein and z_s is the charge on the salt counter-ion.

Electroneutrality on the resin surface dictates that:

$$\Lambda_{IEX} = z_s q_s + (z_p + \sigma)q_p \tag{8}$$

where Λ_{IEX} is the ionic capacity of charged groups on the mixed mode resin and σ is the IEX steric hindrance factor or the number of sterically shielded charges on the resin. Similarly, the total moles of hydrophobic groups on the mixed mode resin must be conserved, thus:

$$\Lambda_{HIC} = c_L + (n + \delta)q_p \tag{9}$$

where Λ_{HIC} is the ligand density of the mixed mode resin and δ is the HIC steric hindrance factor or the number of sterically shielded or inaccessible hydrophobic binding sites on the resin.

Combining Eq. (7)–(9) by replacing c_L and q_s in Eq. (7) gives:

$$K_{eq} = \left(\frac{q_p}{c_p} \right) \left(\frac{z_s c_s}{\Lambda_{IEX} - (z_p + \sigma)q_p} \right)^v \left(\frac{c}{\Lambda_{HIC} - (n + \delta)q_p} \right)^n \left(\frac{1}{\gamma_p} \right) \tag{10}$$

By using the normalized or asymmetric activity coefficient, $\tilde{\gamma}_p = \gamma_p/\gamma_p^{\infty,w}$ and re-arranging Eq. (10), the single component mixed isotherm is obtained:

$$\frac{q_p}{c_p} = \tilde{K}_{eq} \left(\frac{\Lambda_{IEX}}{z_s c_s} \right)^v \left(\frac{\Lambda_{HIC}}{c} \right)^n \left(1 - \frac{(z_p+\sigma)q_p}{\Lambda_{IEX}} \right)^v \left(1 - \frac{(n+\delta)q_p}{\Lambda_{HIC}} \right)^n \tilde{\gamma}_p \tag{11}$$

where $\tilde{K}_{eq} = K_{eq}\gamma_p^{\infty,w}$. In Eq. (11), the terms $1 - (z_p + \sigma)q_p/\Lambda_{IEX}$ and $1 - (n+\delta)q_p/\Lambda_{HIC}$ give the fraction of free ion-exchange and hydrophobic binding sites, respectively, on the mixed mode resin. Eq. (11) can be re-written in terms of the protein binding capacity as:

$$\frac{q_p}{c_p} = \tilde{K}_{eq} \left(\frac{\Lambda_{IEX}}{z_s c_s} \right)^v \left(\frac{\Lambda_{HIC}}{c} \right)^n \left(1 - \frac{q_p}{q_{p,IEX}^{\max}} \right)^v \left(1 - \frac{q_p}{q_{p,HIC}^{\max}} \right)^n \tilde{\gamma}_p \tag{12}$$

where $q_{p,IEX}^{\max} = \Lambda_{IEX}/(z_p + \sigma)$ and $q_{p,HIC}^{\max} = \Lambda_{HIC}/(n + \delta)$.

For mixed mode ligands bearing the same number of each type of functional group, the ligand densities are equal, i.e. $\Lambda_{IEX} = \Lambda_{HIC} = \Lambda$, and likewise are the total number of binding sites of each type, i.e. $(z_p + \sigma) = (n + \delta)$ when the adsorbent is completely saturated. Hence, the mixed mode isotherm in Eq. (12) reduces to:

$$\frac{q_p}{c_p} = \tilde{K}_{eq}(\Lambda)^{v+n} \left(\frac{1}{z_s c_s} \right)^v \left(\frac{1}{c} \right)^n \left(1 - \frac{q_p}{q_{p,MM}^{\max}} \right)^{v+n} \tilde{\gamma}_p \tag{13}$$

where Λ and $q_{p,MM}^{\max}$ are the ligand density and the maximum binding capacity, respectively, of the mixed mode adsorbent. The mixed mode adsorbents examined in this study are functionalized with ligands bearing the same number of electrostatic and hydrophobic interaction groups, hence the above simplification applies.

For multi-component systems, the single component mixed mode isotherm in Eq. (13) can be expressed in terms of the generalized framework presented for HIC and IEX in Eq. (1) as:

$$\frac{q_{p,i}}{c_{p,i}} = A_i \left(1 - \sum_{j=1}^{m} \frac{q_{p,j}}{q_{p,MM,j}^{\max}} \right)^{v_i + n_i} \tag{14}$$

where the initial slope, A_i, of the isotherm for component i in the limiting situation as $q_p \to 0$ is given by:

$$A_i = \lim_{q_p \to 0} \left(\frac{q_p}{c_p} \right) = \Lambda^{(v_i + n_i)} (z_s c_s)^{-v_i} c^{-n_i} \tilde{K}_{eq,i} \tilde{\gamma}_{p,i}$$

$$= \Lambda^{(v_i + n_i)} (z_s c_s)^{-v_i} c^{-n_i} \exp \left(-\frac{\Delta \tilde{G}_p^{\circ}}{RT} + v_i \frac{\Delta G_s^{\circ}}{RT} \right) \tilde{\gamma}_{p,i} \tag{15}$$

The asymmetric activity coefficient is expressed by a suitable activity coefficient model [17,21]:

$$\tilde{\gamma}_{p,i} = \frac{\gamma_{p,i}}{\gamma_{p,i}^{\infty,w}} = \exp(K_{s,i}c_s + K_{p,i}c_{p,i}) \tag{16}$$

where $K_{s,i}$ and $K_{p,i}$ are interaction constants that are specific for the modulator and protein, respectively. In the absence of the ion-exchange mechanism (i.e. for $v = 0$), Eq. (14) reduces to the HIC isotherm, Eqs. (1) and (2). In the absence of hydrophobic interaction (i.e. for $n = 0$), Eq. (14) reduces to the IEX isotherm, Eqs. (1) and (3). Therefore, the proposed model can be seen as an extension of Mollerup's generalized thermodynamic framework to HIC–IEX mixed mode chromatography.

2.3. Isotherm parameters regression

Weighted nonlinear parameters regression was performed by minimization of the sum of squared residuals (SSR) between weighted experimental measurements and the model responses, Eq. (17).

$$SSR = \sum_{k=1}^{m} \left(\frac{q_{p,exp,k} - q_{p,sim,k}}{s_{exp,k}} \right)^2 \tag{17}$$

where $q_{p,exp,k}$ and $q_{p,sim,k}$ are the experimental and simulated solid phase protein concentration at equilibrium, respectively, and $s_{exp,k}$ are the corresponding standard (std) errors or uncertainties.

The fitted mixed mode isotherm parameters included K_{eq}, v, n, K_p, K_s and $q_{p,MM}^{\max}$. The parameters regression involved two main steps. First, better initial estimates of the parameters K_{eq}, v and K_s were obtained by linear regression of the logarithm of the initial slope of the isotherm as a function of salt concentration, Eq. (18).

$$\ln A = \ln \tilde{K}_{eq} + (v + n)\ln(\Lambda) - v \ln(z_s) - n \ln(c) - v \ln c_s + K_s c_s$$

$$= -\frac{\Delta \tilde{G}_p^{\circ}}{RT} + (v + n)\ln(\Lambda) - n \ln(c) + v \left(\frac{\Delta G_s^{\circ}}{RT} + \ln \frac{1}{z_s} \right)$$

$$- v \ln c_s + K_s c_s \tag{18}$$

Then nonlinear weighted regression of all the isotherm parameters was undertaken, using the obtained initial parameter estimates as starting values. Minimization of the SSR was implemented using the constrained optimizer *lsqcurvefit* within MATLAB's optimization toolbox, which is based on the Levenberg-Marquardt method
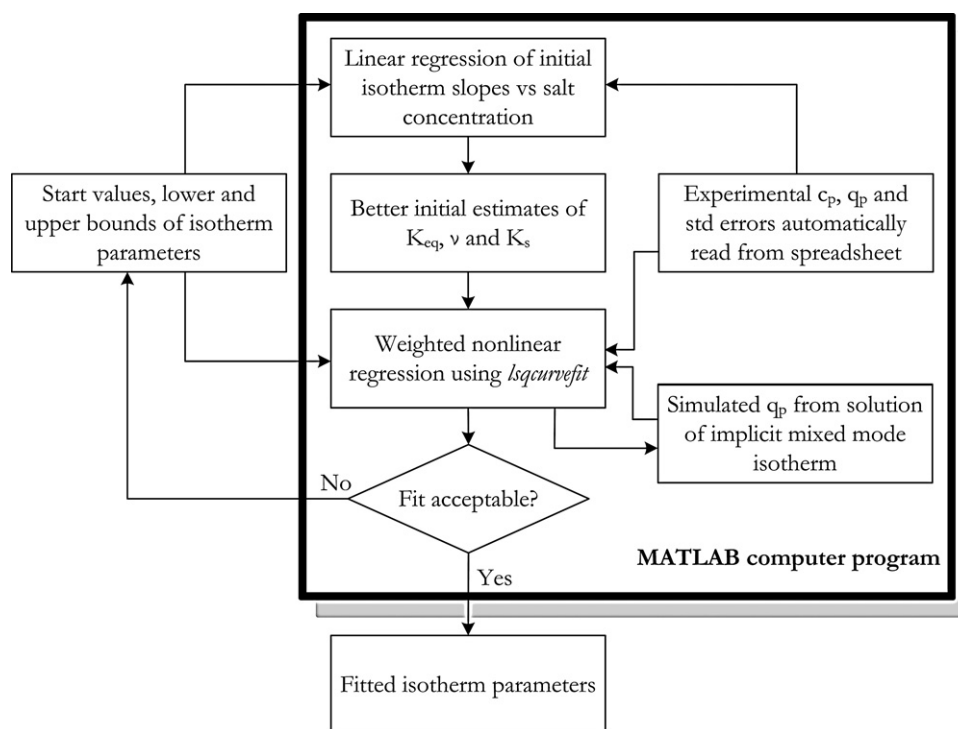
Fig. 1. Overview of parameters regression procedure implemented in MATLAB.

[28]. Since the mixed mode isotherm is implicit in q_p, the nonlinear regression was combined with MATLAB's *fsolve* for numerically solving for q_p. Protein adsorption data obtained for different salt concentrations for each resin–protein–pH combination were fitted together using a single set of isotherm parameters. Given the large amount of experimental data generated by the HT experiments, it was necessary to automate the data handling and parameters regression procedure as much as possible to enable more efficient and fast data processing and analysis, as depicted in Fig. 1.

3. Materials and methods

3.1. Materials

Five model proteins were used in this study. These include albumin from bovine serum (BSA), lysozyme from chicken egg white, albumin from chicken egg white (ovalbumin), alpha-chymotrypsin from bovine pancreas, and amyloglucosidase from *Aspergillus niger*, all purchased from Sigma–Aldrich Chemie, Zwijndrecht, The Netherlands.

Sodium chloride, hydrochloric acid (36–38%), acetic acid, citric acid, disodium hydrogen phosphate and sodium hydroxide were purchased from Mallinckrodt Baker, Deventer, The Netherlands. Ethanol was purchased from Merck, Darmstadt, Germany. Piperazine (99%), Bis-Tris propane (≥99%), triethanolamine (≥98%), N-methylpiperazine (≥99%), BICINE (≥99%) and piperidine (99%) were purchased from Sigma–Aldrich Chemie, Zwijndrecht, The Netherlands.

Four different HIC–IEX mixed mode resins from two different suppliers were investigated. These were PPA HyperCel (phenyl-propylamine) and HEA HyperCel (hexylamine), both donated by Pall Life Sciences, USA, and Capto MMC (2-Benzamido-4-mercaptobutanoic acid) and Capto Adhere (N-benzyl-N-methyl ethanolamine), both purchased from GE Healthcare Benelux, Diegem, Belgium. The ligand structures of all four mixed mode resins are depicted in Fig. 2.

For both PPA HyperCel (PPA) and HEA HyperCel (HEA) from PALL Life Sciences, the beads are made of high porosity cross-linked cellulose with an average particle size of 90 μm, and for both Capto Adhere (ADH) and Capto MMC (MMC) from GE HealthCare, the beads are made of highly cross-linked agarose with an average particle size of 75 μm. HEA bears a hexyl hydrophobic group, while PPA, ADH and MMC each bears the more hydrophobic phenyl group. Additionally, PPA and HEA are weak anion exchangers, bearing an amine group with pK_a ~8, ADH is a strong anion exchange, while MMC is a weak cation exchanger with pK_a ~3. MMC and ADH are both designed with hydrogen bonding groups close to the ion-
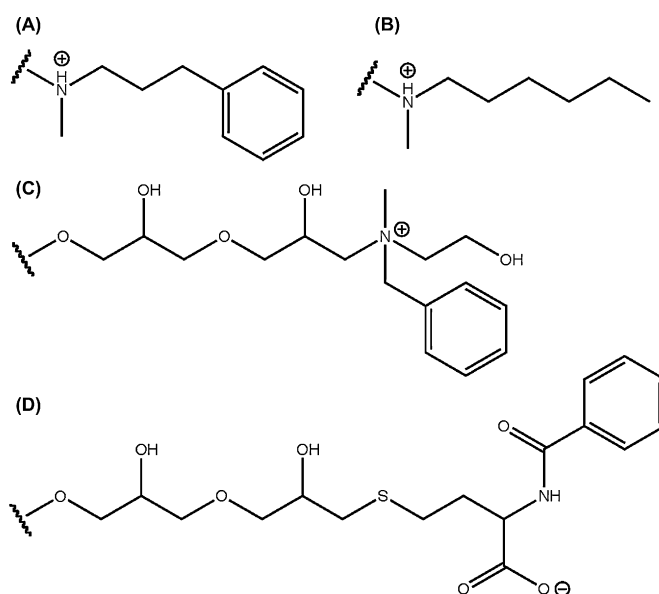

Fig. 2. Ligand structures of mixed mode resins used in this study. (A) PPA HyperCel (phenylpropylamine); (B) HEA HyperCel (hexylamine); (C) Capto Adhere (N-benzyl-N-methyl ethanolamine); (D) Capto MMC (2-benzamido-4-mercaptobutanoic acid).

Table 1
Characteristics of mixed mode resins used in this study.

Resin	Average ligand density (mmol/L gel)[a]	Dispensed resin mass (mg)	Settled resin volume (μL)
PPA	65	79.50 ± 0.12	48.7 ± 1.2
HEA	67	77.950 ± 0.094	50.0 ± 2.0
ADH	105	76.908 ± 0.086	50.0 ± 2.0
MMC	80	75.741 ± 0.087	51.2 ± 1.2

[a] Provided by the resin suppliers.

exchange group, to provide additional interactions by hydrogen bonding. The average ligand densities of the mixed mode resins are summarized in Table 1.

3.2. Equipments

A 12 × 300 Pipetman Concept Multichannel pipette from Gilson was used to load the resin into the plate wells. A JANUS Robotic Workstation from Perkin-Elmer was used for liquid manipulations. It was equipped with a Varispan 8-fixed tips arm and a 96-tip Modular Dispense Technology (MDT) dispensing arm. Each tip of the Varispan arm can transfer a different volume of liquid but each tip of the MDT arm transfers the same volume of liquid. The Varispan arm was used for equilibration, protein binding and dilution steps. The fixed tips were washed using the standard cleaning protocol before each new liquid could be dispensed and after each dispense if the tip contacted the liquid in the well. The MDT arm was used for the regeneration and storage steps. The automated workstation was controlled by WinPrep for Janus. A Synergy 2 Multi-Mode Microplate Reader from BioTek with Gen5 software from BioTek was used for absorbance measurements. MultiScreen Deep Well Solvinert filter plates (catalog number: MDRPN0410) from Millipore were used. They had hydrophobic PTFE membranes with pore size of 0.45 μm.

3.3. Buffers and solutions preparation

Buffers made with Bis-Tris, MES, BICINE, piperazine, N-methylpiperazine and acetic acid were prepared by dissolving the appropriate amount of chemical in Milli-Q water, adjusting the pH to the desired value with 2 M HCl or 2 M NaOH and adjusting the liquid level to the desired volume with Milli-Q water. pH 6.5 was achieved using 50 mM Bis-Tris buffer for PPA, HEA and ADH resins and 50 mM MES for MMC. pH 9.0 was achieved using 50 mM BICINE buffer for all investigated resins. Buffers made with a mix of citric acid and Na_2HPO_4 were prepared by mixing a stock solution of 0.1 M citric acid with a stock solution 0.1 M Na_2HPO_4 at a given ratio depending on the desired pH (for pH 5.5, citric acid:Na_2HPO_4 = 43.1:56.9 was used; for pH 4.5, citric acid:Na_2HPO_4 = 54.6:45.4 was used). The pH was adjusted by adding more of the citric acid stock solution if it was higher than desired, or Na_2HPO_4 stock solution if it was lower than desired.

NaCl salt solutions were prepared by dissolving the appropriate amount of salt in the corresponding buffer, adjusting the pH to the desired value with 2 M HCl or 2 M NaOH and adjusting the liquid level to the desired volume with the corresponding buffer.

Protein solutions were made by dissolving the appropriate amount of protein in the corresponding buffer without NaCl, adjusting the pH with 2 M HCl or 2 M NaOH and adjusting the volume with the corresponding buffer. All buffers and solutions were prepared using Milli-Q water and were filter-sterilized using 0.45 μm filters.

3.4. Isotherm measurement

The adsorption isotherm of a solute gives the equilibrium concentrations of that solute adsorbed at different concentrations in the liquid. Protein adsorption isotherms were obtained by contact-

ing known amounts of protein with a known amount of resin and measuring the protein concentration in the liquid phase after equilibrium had been reached. The adsorbed amount was calculated by mass balance. Different amounts of protein were used in order to get the complete adsorption curve.

Prior to the protein binding experiments, protein calibration curves were prepared from measured UV absorbances (at 280 nm) of serial dilutions of 2 mg/mL stock solutions of each protein, A correction was done by subtracting the UV absorbance contribution of a protein-free solution of equivalent buffer composition. Protein binding experiments were carried out in 96-deepwell filter plates, preloaded with resin. Each plate was used to measure adsorption isotherms for one resin-protein-pH combination at different salt concentrations. The plates were configured such that each carried six adsorption isotherms corresponding to the six salt concentrations investigated (0 M, 0.4 M, 0.8 M, 1.2 M, 1.6 M and 2.0 M), and each isotherm was composed of eight protein data points measured in duplicates (6 × 8 × 2 = 96). The resin was loaded into the 96-deepwell filter plate once and was regenerated in the plate after an isotherm measurement. It was reused for other proteins or pH conditions. The protein concentration after equilibration was measured by UV adsorbance at 280 nm. The liquid phase supernatant was collected by centrifugation in a 96-deepwell collector plate and was then transferred to 96-well UV plates for reading at 280 nm in a UV plate reader. The measured UV signals of the protein samples were similarly corrected using the UV absorbance of protein-free solutions of equivalent buffer compositions. Dilutions were performed when the recorded adsorbance was outside the range of the calibration curve. The main steps involved in high throughput batch uptake experiments include resin dispensing and characterization, equilibration, protein binding, and resin regeneration and storage or re-equilibration for the next round of batch adsorption experiments. Each step is described in a separate subsection below.

3.5. Resin dispensing and characterization

3.5.1. Resin dispensing

The resin was obtained in a 70–75% (v/v) slurry. The container was agitated to suspend all particles and the mixture poured into a reagent reservoir for multi channel pipette placed on an orbital shaker. Just before pipetting, the orbital shaker was switched on and the slurry was stirred with a tip until all the particles were suspended. 75 μL of resin was manually dispensed in the 96-deepwell filter plate using an electronic 12-arm multichannel micropipette set on repetitive mode to aspirate 300 μL of the resin slurry and dispense 75 μL of the settled resin at the first command after a settling time of 30 min. Just before dispensing into the 96-deepwell filter plate, the tips orifices were quickly dipped in the supernatant of the resin slurry reservoir to rehydrate possible dried resin at the bottom of the tips. After loading, the remaining resin in the tips was put back in the resin slurry reservoir. This was repeated until all the deepwell plates were loaded.

3.5.2. Settled resin volume

Twelve 0.5 mL pre-weighed micro-tubes were loaded in the same way. The mass of dispensed material was measured and the inter-tip dispensed mass error was calculated. The settled volume of dispensed resin was measured by centrifuging the dispensed material in the calibrated micro-tubes.

3.5.3. Liquid hold-up volume

The resin is never completely dry after centrifugation. Hence, the determination of this residual amount of liquid – the liquid holdup volume – is necessary to correct the mass balance used to calculate the concentration of adsorbed protein. The liquid hold-up volume was measured by contacting the resin with a solution of

known concentration of NaCl for 10 minutes without agitation at 21 °C. Then the plate was centrifuged (2900 × g, 21 °C, 5 min), the flow-through collected and its conductivity measured. This cycle was repeated until the conductivity of the flow-through was equal to the one of the NaCl solution. The resin was contacted with a defined volume of MilliQ water overnight at 21 °C without agitation. After contacting, the plate was centrifuged, the flow-through was collected and its conductivity measured. The salt concentration was calculated using a calibration curve made for the conductimeter and probe used. The hold-up volume was calculated by mass balance:

$$c_{s,initial}V_H = c_{s,final}(V_H + V_W) \Leftrightarrow V_H = \frac{c_{s,final} \cdot V_W}{c_{s,initial} - c_{s,final}} \qquad (19)$$

where V_H is the liquid hold-up volume, $c_{s,initial}$ is the known concentration of NaCl, V_W is the known volume of MilliQ water used to contact the resin overnight and $c_{s,final}$ is the concentration of NaCl after the overnight contacting.

3.6. Equilibration

The equilibration step prepares the resin to the conditions desired for the protein binding step. A mixture of buffer 1 (buffering agent only) and buffer 2 (buffering agent plus 4 M NaCl) was dispensed into the wells to achieve the desired conditions. The total dispensed volume was 1000 µL per well. After dispensing, the plates were placed on deepwell collector plates and covered. The stack was incubated at 150 rpm and 21 °C for 30 min. The plates were centrifuged at 4000 × g and 21 °C for 5 min and the equilibration step was repeated.

3.7. Protein binding

Protein loading was done by the liquid handling robot using the varispan 8 needles arm. The desired protein and salt concentration was achieved by mixing three stock solutions. The first solution was the buffering agent only (buffer 1). The second solution was the buffering agent with a salt concentration that was twice the highest desired salt concentration (buffer 2). The third solution was the protein dissolved into buffer 1 at a concentration that was twice the highest desired protein concentration. Buffer 1 and buffer 2 were loaded with the needles always above the resin or liquid level, so no contamination of the needles could occur. The needles were washed before each buffer loading step. The protein solution was loaded 3 mm below the liquid surface to ensure that all the solution was dispensed into the well. The needles were washed after each dispense. The total dispensed volume per well was 334 µL.

The loaded 96-deepwell filter plates were placed on top of pre-weighed collector plates. The 96-deepwell filter plate was sealed with a sheet of parafilm to prevent evaporation and covered with a plastic lid. The stack was weighed and then placed into the appropriate casing that fitted the fixation system in the orbital shaking incubator. The incubator was set at 150 rpm and 21 °C and the plates were let incubating overnight. After overnight incubation, the stack was re-weighed to check for liquid evaporation. The deepwell collector plates were equally re-weighed to detect possible leaks. The plates were placed on new deepwell collector plates and then centrifuged.

The centrifuged liquid was dispensed into 96-UV measurement plates for absorption measurement using the varispan 8 needles arm. The needles were washed after each dispense. The undiluted plates were read at 280 nm and dilutions were performed if the UV absorbance was outside the linear range of the protein calibration curve, prepared for each model protein. Dilutions were performed using the varispan 8 needles arms. A combination of buffer 1 and buffer 2 was used as diluent so the salt composition and pH remained unchanged.

3.8. Resin regeneration and storage

3.8.1. Resin regeneration

The regeneration step cleans the resin of bound proteins so it can be reused for another isotherm recording. 1000 µL of regeneration solution was dispensed using the 96-tips arm. The regeneration solution was 0.1 M acetic acid for Capto Adhere, PPA and HEA HyperCel and 2 M NaCl at pH 11 for Capto MMC. After dispensing, the plates were placed on deepwell collector plates and covered. The stack was incubated at 150 rpm and 21 °C for 30 min. After incubation, the plates were centrifuged and the absorbance of the flow-through at 280 nm were recorded. This step was repeated until the absorbance was close to that of the protein-free blank. On average, four resin regeneration cycles were sufficient.

3.8.2. Resin storage

The composition of the storage solution was 20% (v/v) ethanol for Capto Adhere and Capto MMC resin and 20% (v/v) ethanol and/or 1 M NaCl for PPA and HEA HyperCel resins. 1000 µL of storage solution was dispensed using the 96-tips arm. If the plate needed to be stored, 1000 µL of the storage solution was added in each well and the plate was placed on a collector plate and covered. The plates were stored at 4 °C.

3.9. Determination of equilibrium protein concentration

During the static binding experiment, a known amount of protein was contacted with the resin until the liquid phase and the solid phase concentrations were at equilibrium. The final protein concentration in the liquid phase in equilibrium with the solid was determined from the protein concentration in the diluted supernatant (obtained from the calibration curve) and the dilution factor.

The protein concentration in the solid phase in equilibrium with the liquid was calculated from the mass balance of the total amount of protein dispensed into each well, which at equilibrium is distributed between the solid phase and the liquid phase:

$$c_{p,load}V_{load} = q_{p,eq}V_{resin} + c_{p,eq}(V_{load} + V_H) \Leftrightarrow q_{p,eq}$$
$$= \frac{c_{p,load}V_{load} - c_{p,eq}(V_{load} + V_H)}{V_{resin}} \qquad (20)$$

where V_{load} is the pre-defined volume of liquid (protein plus buffer solutions) dispensed into each well and $c_{p,load}$ is the corresponding protein concentration, $q_{p,eq}$ is the solid phase protein concentration in equilibrium with the liquid phase and V_{resin} is the volume of resin in each well. The term $c_{p,load}V_{load}$ gives the total amount of protein dispensed into the well. The term $q_{p,eq}V_{resin}$ gives the amount of protein adsorbed at equilibrium and $c_{p,eq}(V_{load} + V_H)$ gives the liquid phase protein amount at equilibrium, taking into account the liquid hold-up volume. The standard errors on the isotherm data were determined by the uncertainty propagation analysis method documented by the Joint Committee for Guides in Metrology (JCGM) [29].

4. Results and discussion

4.1. Resin and protein characteristics

The same dispensed resin slurry volume (75 µL) was used for all four mixed mode resins examined. The mean values of the mass and settled volume of the dispensed materials are summarized in

Table 2
Properties of model proteins used in this study.

Protein	M_r (kDa)[a]	pI[b]
Bovine serum albumin (BSA)	66.4	5.5[c]
Lysozyme (LYS)	14.3	11.0
Ovalbumin (OVA)	44.3	4.9
Amyloglucosidase (AMY)	97.0	3.9
α-Chymotrypsin (CHY)	25.0	8.7

[a] M_r values were obtained from the supplier (www.sigmaaldrich.com) using the product name and source.
[b] Except otherwise indicated, the pI values are those from titration curves calculated using amino acid pK_as from the 3D structures of the proteins.
[c] Obtained from Refs. [38,39].

Table 1. The results show that repeated measurements of the dispensed mass and settled resin volume were very consistent, within the standard errors of the measurements.

Measured resin liquid hold-up volumes were ∼7–8% of the total volume dispensed per well (334 μl). The hold-up volume was used in Eq. (20) for calculating the adsorbed phase protein concentration at equilibrium. Its negligence would have led to a systematic error that would slightly over estimate the calculated adsorbed phase protein concentration.

The model proteins used in this study span a broad range of molecular masses and iso-electric points (pIs) as shown in Table 2.

4.2. Expected trends of mixed mode protein binding strength with pH and salt concentration

The salt concentration or ionic strength and solution pH are two important factors that influence protein adsorption by electrostatic and hydrophobic interactions on mixed mode resins and the relative contribution of each interaction to the net protein binding strength. Before considering the measured protein adsorption isotherms, a qualitative analysis of the expected trends of the mixed mode protein binding strength with pH and salt concentration is first considered, as depicted in Fig. 3.

4.2.1. Effect of pH on mixed mode protein binding strength

The solution pH affects the charge states of the protein and the resin and therefore has a strong influence on the strength of electrostatic protein–ligand interactions. This is schematically depicted in

Fig. 3a for a weak anion exchange mixed mode ligand. The parameters of interest here are the pI of the protein and the pK_a of the charged group on the ligand. By varying the solution pH relative to the pI of the protein and the pK_a of the ligand, the net charges on the protein and the ligand can be manipulated as shown in Fig. 3a. At pH values below the pI, the protein and ligand become similarly charged and so experience electrostatic charge repulsion. This phenomenon is commonly exploited to achieve protein desorption from mixed mode resins [7]. At pH values close to or equal to the pI, the protein loses most or all of its net charge and so hydrophobic interactions are expected to be dominant. At pH values above the pI of the protein and below the pK_a of the ligand, the strength of electrostatic protein interaction increases with increasing pH. When the pH is increased above the pK_a (or below the pK_a in the case of a weak cation exchanger), the ligand gradually loses its net charge thereby weakening the electrostatic protein interactions.

4.2.2. Effect of salt concentration on mixed mode protein binding strength

Protein adsorption on mixed mode resins occurs through a combination of electrostatic and hydrophobic interactions. Salt concentration has opposing effect on these interactions, with electrostatic interactions decreasing with increasing salt concentration while hydrophobic interactions increase as schematically is depicted in Fig. 3b. When the ligand and protein are oppositely charged, electrostatic protein–ligand interactions dominate at low salt concentrations and decrease with increasing salt concentration until some intermediate salt concentration is reached where the opposing tendencies of the electrostatic and hydrophobic interactions balance each other, resulting in minimal protein binding strength. As the salt concentration increases beyond the minimum point, hydrophobic interactions become dominant. This salt-tolerant behavior gives rise to a U-shaped protein binding strength as shown in Fig. 3b.

Salt-tolerant protein adsorption has been observed even under conditions where there is electrostatic repulsion between the protein and the ligand [15,30]. In this case, electrostatic protein–ligand interactions are mainly driven by the heterogeneous charge distribution on the surface of the protein which creates oppositely charged regions or patches on the protein with respect to the ligand, irrespective of the fact that the net charge of the protein is of the same sign as that of the adsorbent. In this situation, protein
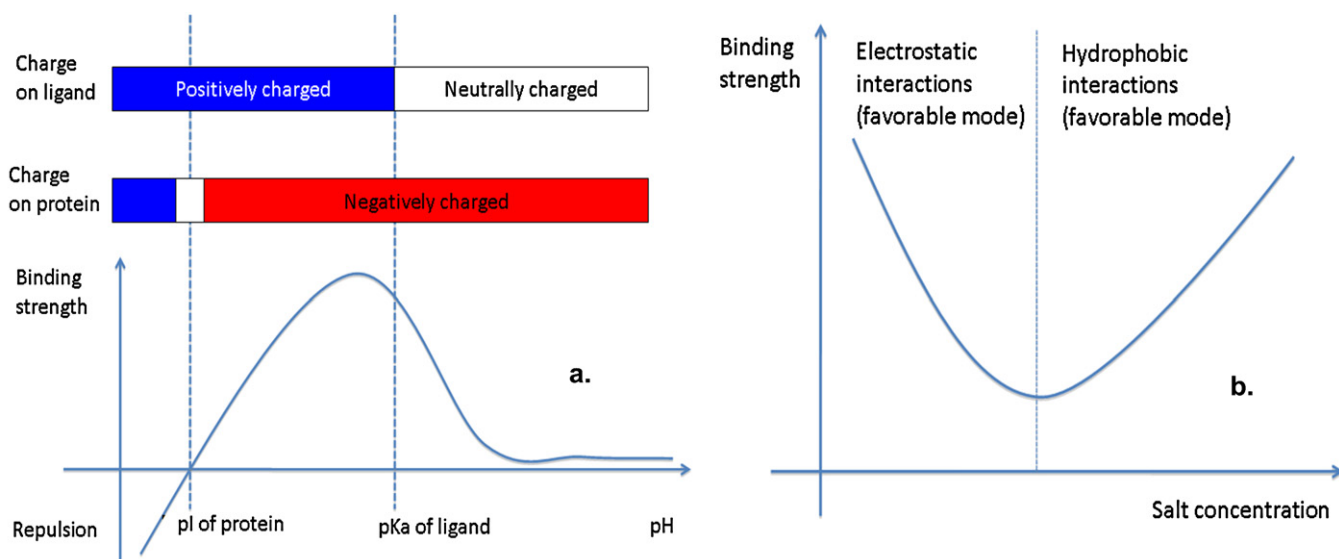

Fig. 3. Schematic representation of the effect of pH and salt concentration on mixed mode protein binding strength. (a) Effect of pH on electrostatic interactions. (b) Effect of salt concentration on electrostatic and hydrophobic interactions.

Table 3
Resin–protein–pH combinations investigated.

Resin	Protein and pH				
	BSA	LYS	OVA	AMY	CHY
PPA	6.5, 5.5	9.0, 6.5	6.5, 4.5	6.5, 4.5	9.0
HEA	6.5, 4.5	9.0, 6.5	6.5, 4.5	6.5, 4.5	9.0
ADH	6.5, 5.5, 4.5	9.0, 6.5	6.5, 4.5	6.5, 4.5	9.0, 6.5
MMC	6.5, 5.5, 4.5	9.0, 6.5	–	–	–

adsorption is said to be 'patch-controlled' [15,30].

4.3. Protein adsorption isotherms

Protein adsorption isotherms were obtained for the resin, protein and pH combinations shown in Table 3, and for six different NaCl concentrations (0, 0.4, 0.8, 1.2, 1.6 and 2 M).
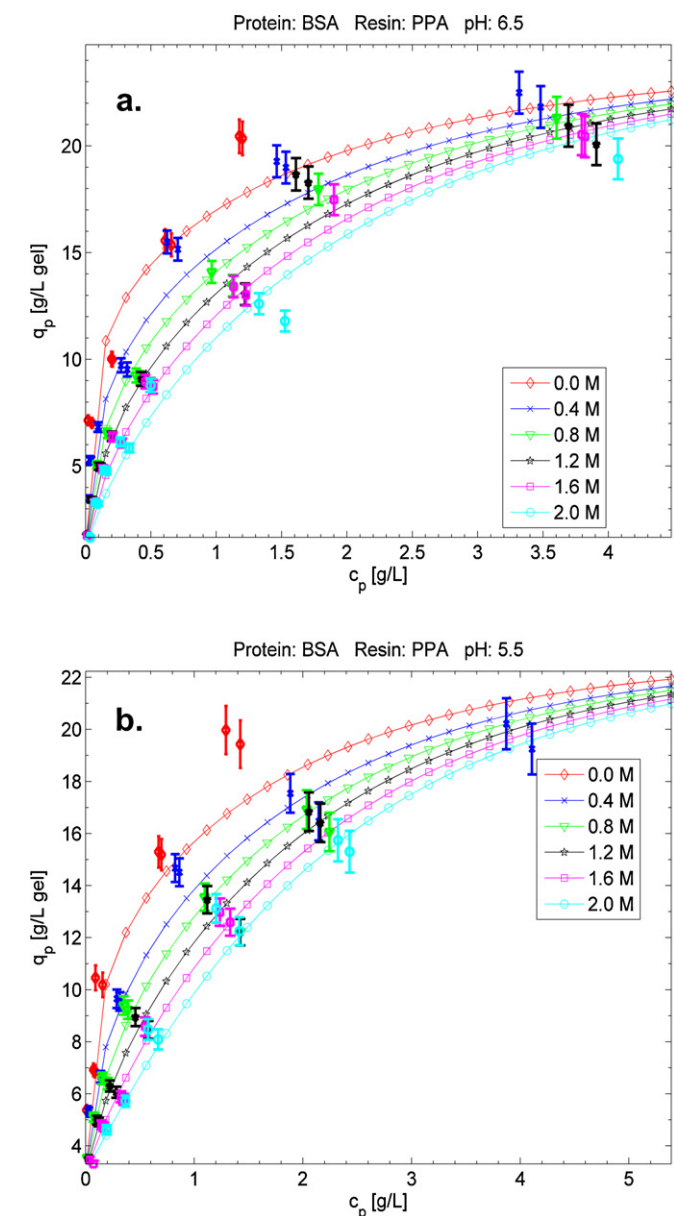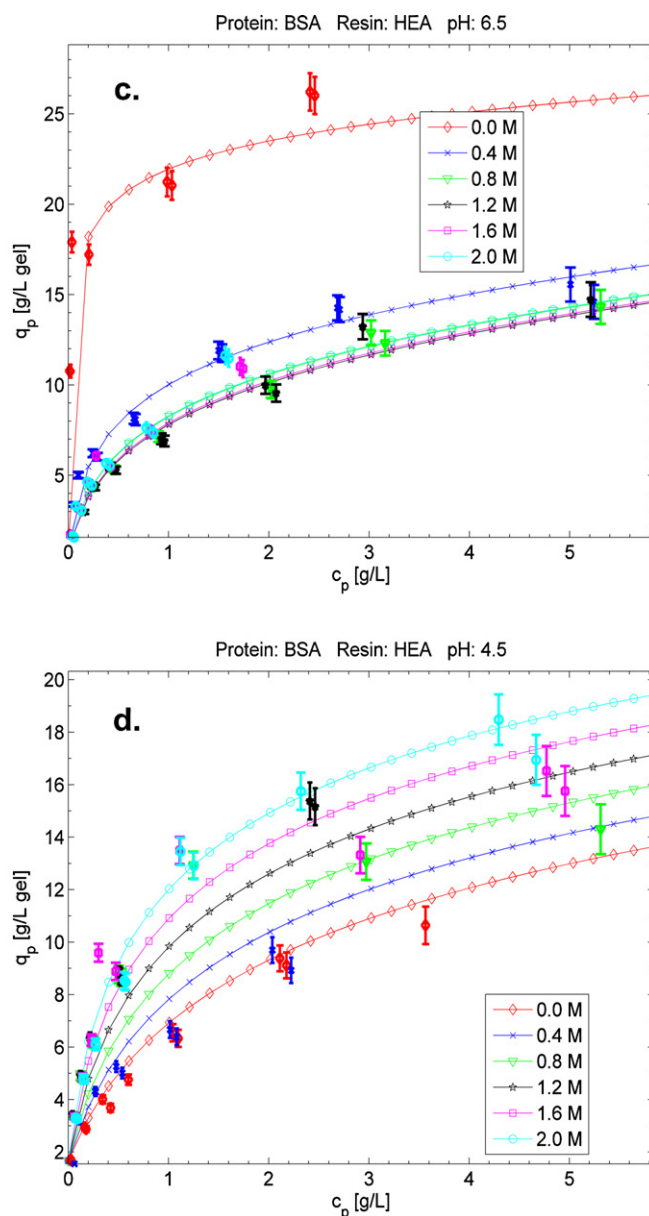
The adsorption isotherms as well as the fitted results from the mixed mode isotherm formalism in Eq. (13) are presented in Figs. 4–10. In general, the adsorption isotherms show the typical saturation behavior of single protein adsorption on mixed mode adsorbents [8,14,24,25].

A clearly visible pattern observed with protein adsorption isotherms of each resin–protein–pH combination at the different salt concentrations is that the equilibrium adsorbed phase protein concentration and the corresponding liquid phase protein concentration fall on a straight line when the same starting protein concentration ($c_{p,load}$) was used, with a negative slope and intercepts given by the mass balance in Eq. (20), whereby the X-axis intercept corresponds to the starting protein concentration.

4.4. Mixed mode isotherm parameters

The regressed isotherm parameters of the different resin–protein–pH combinations, along with their standard errors,

Fig. 4. Effects of NaCl salt concentration, pH and type of ligand on the adsorption isotherms of BSA on PPA and HEA. (a) PPA, pH 6.5; (b) PPA, pH 5.5; (c) HEA, pH 6.5; (d) HEA, pH 4.5. Symbols with error bars represent experimental data and the solid lines represent fitted results from the mixed mode isotherm in Eq. (13). The different NaCl concentrations are given by the colour legends. (For interpretation of the references to colour in this figure legend, the reader is referred to the web version of the article.)
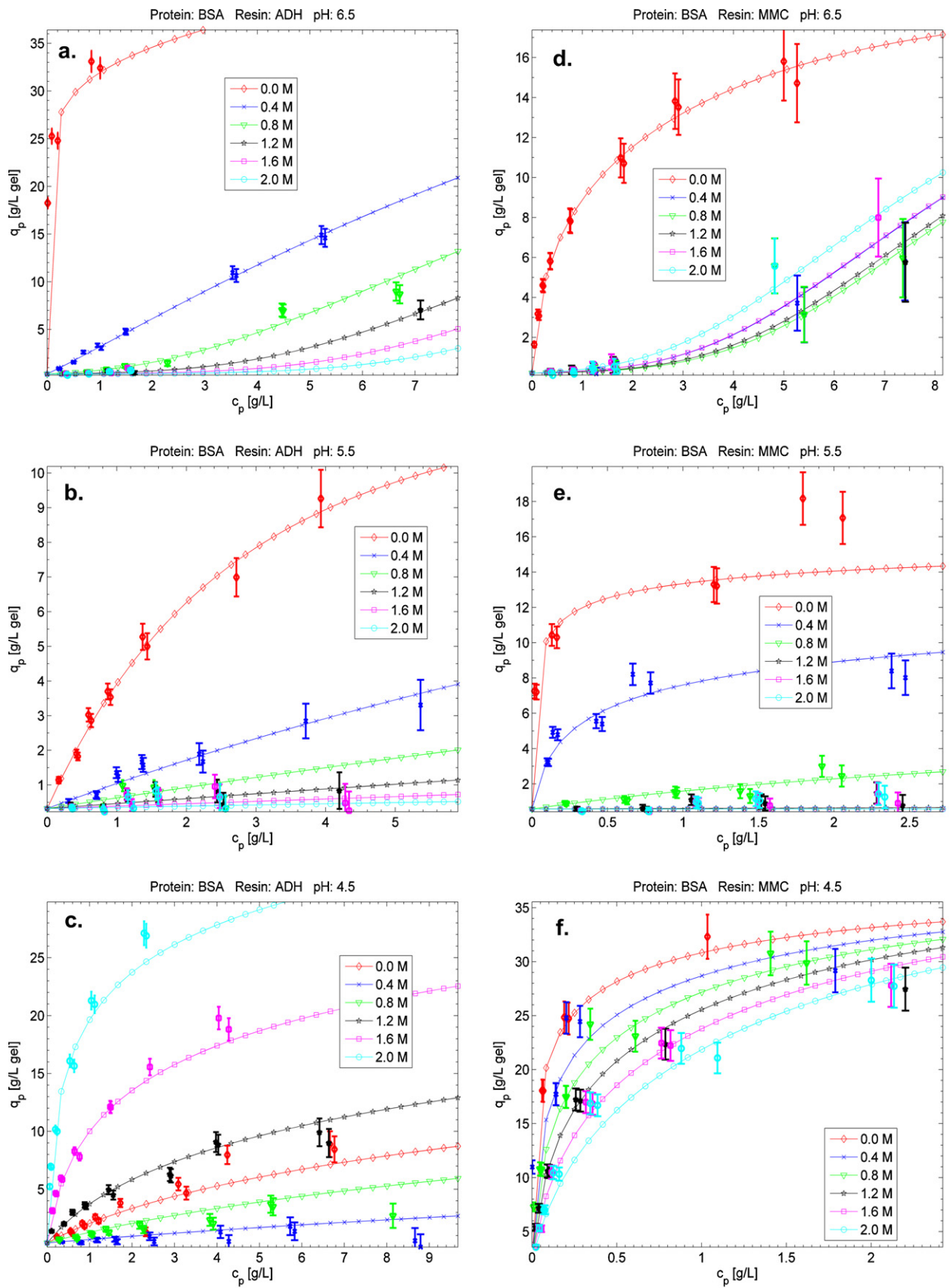
Fig. 5. Effects of NaCl salt concentration, pH and type of ligand on the adsorption isotherms of BSA on ADH and MMC. (a) ADH, pH 6.5; (b) ADH, pH 5.5; (c) ADH, pH 4.5; (d) MMC, pH 6.5; (e) MMC, pH 5.5; (f) MMC, pH 4.5. Symbols with error bars represent experimental data and the solid lines represent fitted results from the mixed mode isotherm in Eq. (13). The different NaCl concentrations are given by the colour legends. (For interpretation of the references to colour in this figure legend, the reader is referred to the web version of the article.)

Fig. 6. Effects of NaCl salt concentration, pH and type of ligand on the adsorption isotherms of lysozyme (LYS) on PPA and HEA. (a) PPA, pH 9.0; (b) PPA, pH 6.5; (c) HEA, pH 9.0; (d) HEA, pH 6.5. Symbols with error bars represent experimental data and the solid lines represent fitted results from the mixed mode isotherm in Eq. (13). The different NaCl concentrations are given by the colour legends. (For interpretation of the references to colour in this figure legend, the reader is referred to the web version of the article.)
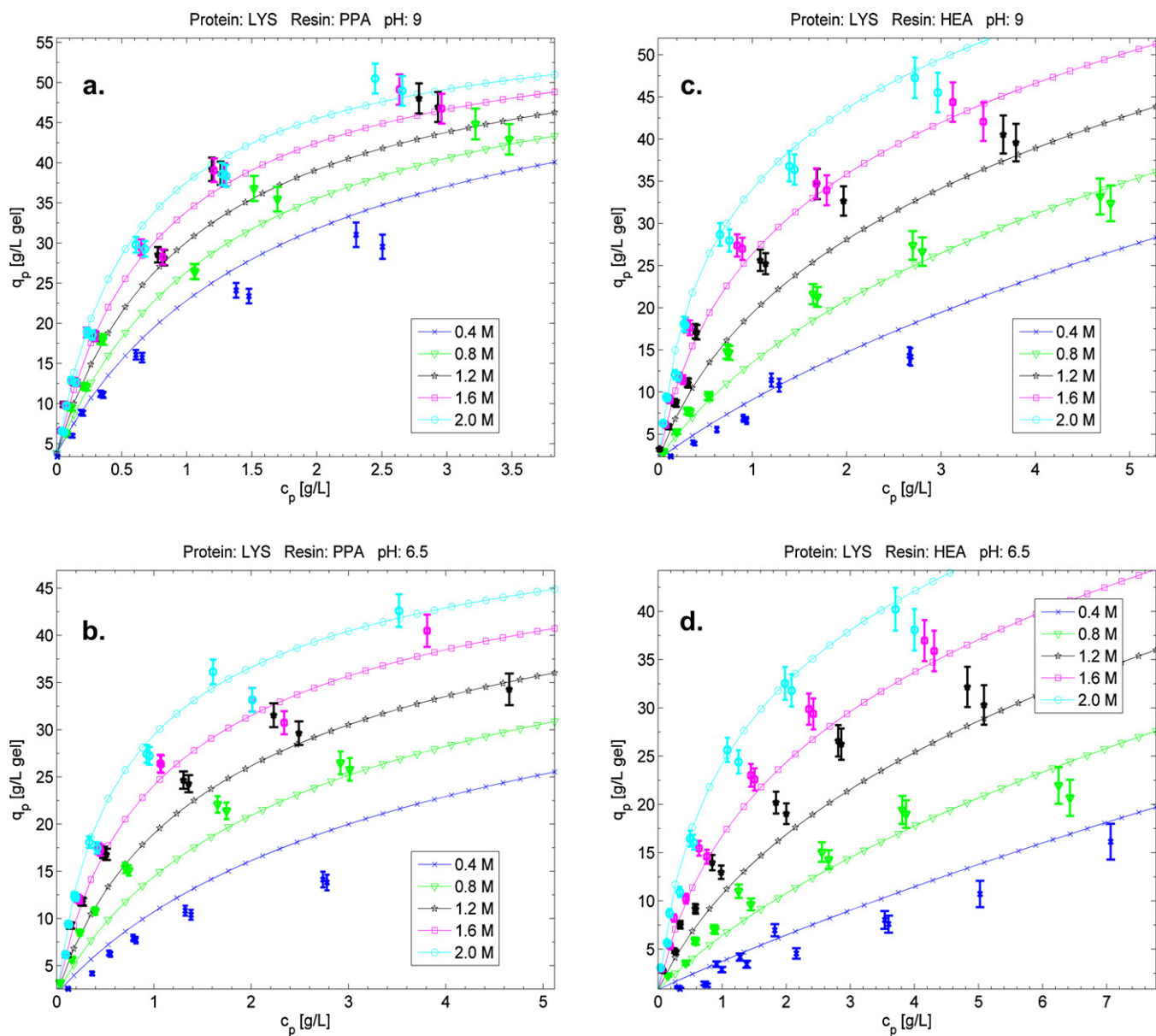
are presented in Table 4. The parameters enable a more quantitative analysis of the observed isotherm behaviors. As expected, the solution pH has a strong influence on the effective charge of the protein (z_p). The generally observed trend is that at solution pH favorable for electrostatic interactions to occur (i.e. pH > pI for PPA, HEA and ADH or pH < pI for MMC), the protein possesses an effective charge greater than zero (i.e. $z_p > 0$), e.g. PPA-BSA-6.5, HEA-BSA-6.5, ADH-OVA-6.5, MMC-LYS-9.0, MMC-LYS-6.5. As the pH moves towards and across the pI of the protein, the effective charge sharply decreases. For example, the effective charge of OVA drops to nearly zero (taking into account the standard errors) as the pH crosses the pI of OVA (pI ∼4.9). Likewise, LYS possesses almost no effective charge on PPA, HEA and ADH below its pI, and its effective charge on MMC decreases sharply in going from pH 6.5 to pH 9.0, as the pI of LYS is approached (pI ∼11.0). However, there are cases where electrostatic interactions were observed ($z_p > 0$) at solution pH unfavorable for these interactions to occur (below the

pI for PPA, HEA and ADH or above the pI for MMC). For example, ADH-BSA-4.5, MMC-BSA-6.5, and ADH-CHY-6.5. The occurrence of electrostatic interactions under unfavorable pH conditions can be attributed to mechanisms such as the patch-controlled protein adsorption described earlier. No correlation could be found between the solution pH and the number of hydrophobic ligands (n) nor the equilibrium constant (K_{eq}).

The prevalent mixed mode interaction mechanism under a given solution condition can quite easily be deduced from the effective charge (z_p) and the number of interacting hydrophobic ligands (n). For example, if $z_p \approx 0$, then the hydrophobic interaction mode is dominant and so the protein binding capacity should increase with increasing salt concentration (e.g. isotherms of LYS on PPA, HEA and ADH in Figs. 6 and 7). On the other hand, if $n \approx 0$, then the electrostatic interaction mode is dominant and the protein binding capacity should decrease with increasing salt concentration (e.g. MMC-LYS-9.0 and MMC-LYS-6.5 in Fig. 7). If both
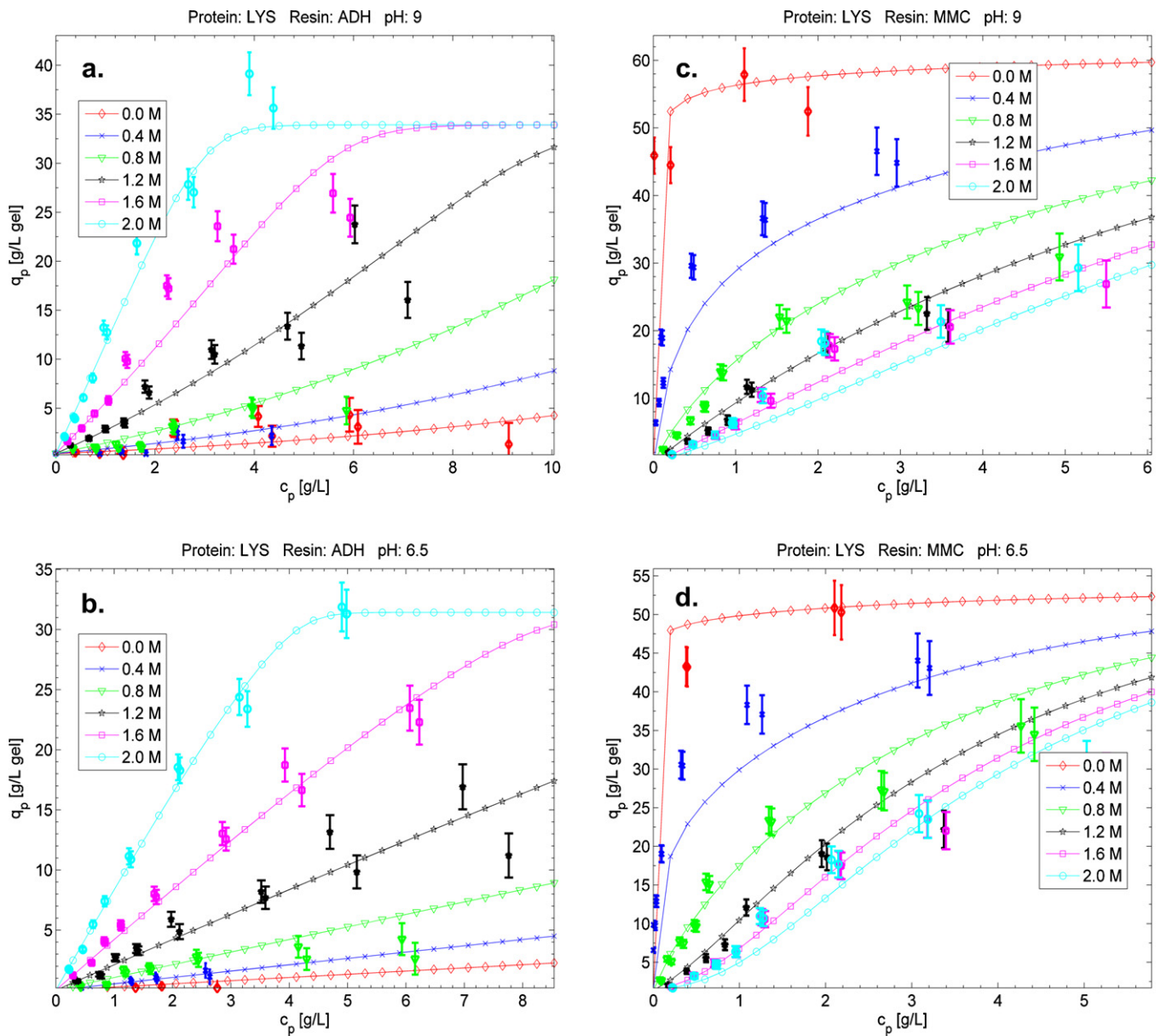
Fig. 7. Effects of NaCl salt concentration, pH and type of ligand on the adsorption isotherms of lysozyme (LYS) on ADH and MMC. (a) ADH, pH 9.0; (b) ADH, pH 6.5; (c) MMC, pH 9.0; (d) MMC, pH 6.5. Symbols with error bars represent experimental data and the solid lines represent fitted results from the mixed mode isotherm in Eq. (13). The different NaCl concentrations are given by the colour legends. (For interpretation of the references to colour in this figure legend, the reader is referred to the web version of the article.)

z_p and n are non-zero, then the mixed mode protein adsorption is salt-tolerant, although this salt-tolerance may or may not be visible on the isotherms within the investigated salt concentration range. Therefore, a visual inspection of the isotherms as a function of salt concentration is alone insufficient to conclude the presence or absence of salt tolerant protein adsorption. Neither can a good estimate of the salt concentration at which minimum protein adsorption occurs be deduced by visual inspection of the isotherms.

From the derived mixed mode isotherm model in Eq. (13), however, the salt concentration at which minimum protein binding occurs can be precisely calculated by taking the derivative of the adsorbed phase protein concentration (q_p) as a function of salt concentration (c_s). The analytical derivative is given by:

$$\frac{dq_p}{dc_s} = \frac{(K_s - (\nu/c_s))q_p}{1 + (\nu + n)(q_p/(q_{p,MM}^{max} - q_p))} \tag{21}$$

At the turning point, where $dq_p/dc_s = 0$, the following condition holds:

$$\left(K_s - \frac{\nu}{c_{s,min}}\right) q_p = 0 \Leftrightarrow K_s = \frac{\nu}{c_{s,min}} \Leftrightarrow c_{s,min} = \frac{\nu}{K_s} \tag{22}$$

Therefore under conditions where the adsorbed phase protein concentration is greater than zero, i.e. $q_p > 0$, the minimum protein binding capacity occurs at a threshold salt concentration given by Eq. (22), where $c_{s,min}$ is the threshold salt concentration at which minimum protein adsorption on the mixed mode adsorbent occurs, and K_s is the salt–protein interaction parameter. Calculated values of the threshold salt concentrations are tabulated in Table 4 and they are in excellent agreement with the protein adsorption isotherms presented in Figs. 4–10.

Obviously, for $z_p \approx 0$, the minimum protein adsorption occurs at zero salt concentration. When the effective charge and the salt–protein interaction parameter (K_s) are both greater than zero,
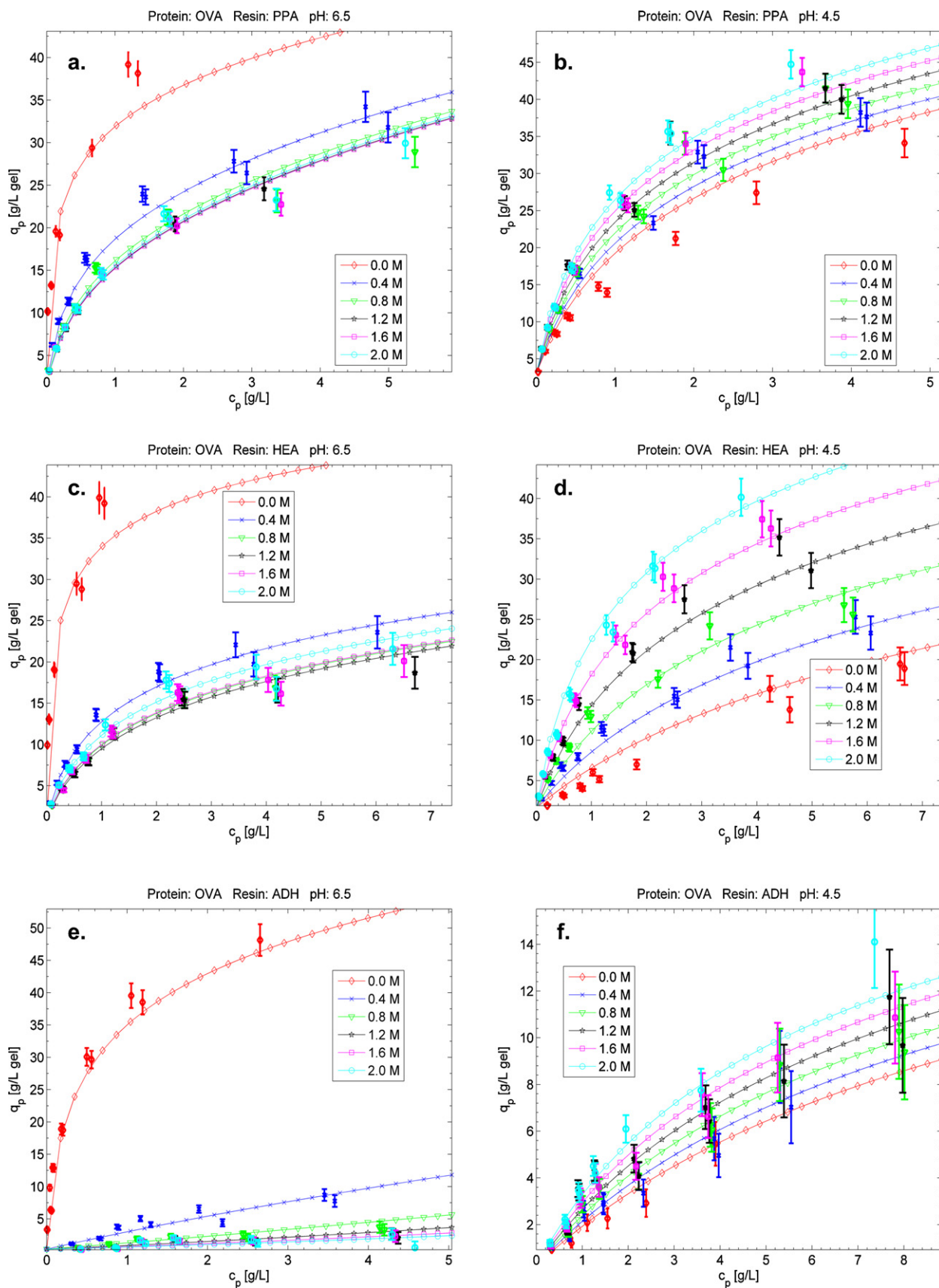
Fig. 8. Effects of NaCl salt concentration, pH and type of ligand on the adsorption isotherms of ovalbumin (OVA) on PPA, HEA and ADH. (a) PPA, pH 6.5; (b) PPA, pH 4.5; (c) HEA, pH 6.5; (d) HEA, pH 4.5; (e) ADH, pH 6.5; (f) ADH, pH 4.5. Symbols with error bars represent experimental data and the solid lines represent fitted results from the mixed mode isotherm in Eq. (13). The different NaCl concentrations are given by the colour legends. (For interpretation of the references to colour in this figure legend, the reader is referred to the web version of the article.)

Fig. 9. Effects of NaCl salt concentration, pH and type of ligand on the adsorption isotherms of amyloglucosidase (AMY) on PPA, HEA and ADH. (a) PPA, pH 6.5; (b) PPA, pH 4.5; (c) HEA, pH 6.5; (d) HEA, pH 4.5; (e) ADH, pH 6.5; (f) ADH, pH 4.5. Symbols with error bars represent experimental data and the solid lines represent fitted results from the mixed mode isotherm in Eq. (13). The different NaCl concentrations are given by the colour legends. (For interpretation of the references to colour in this figure legend, the reader is referred to the web version of the article.)
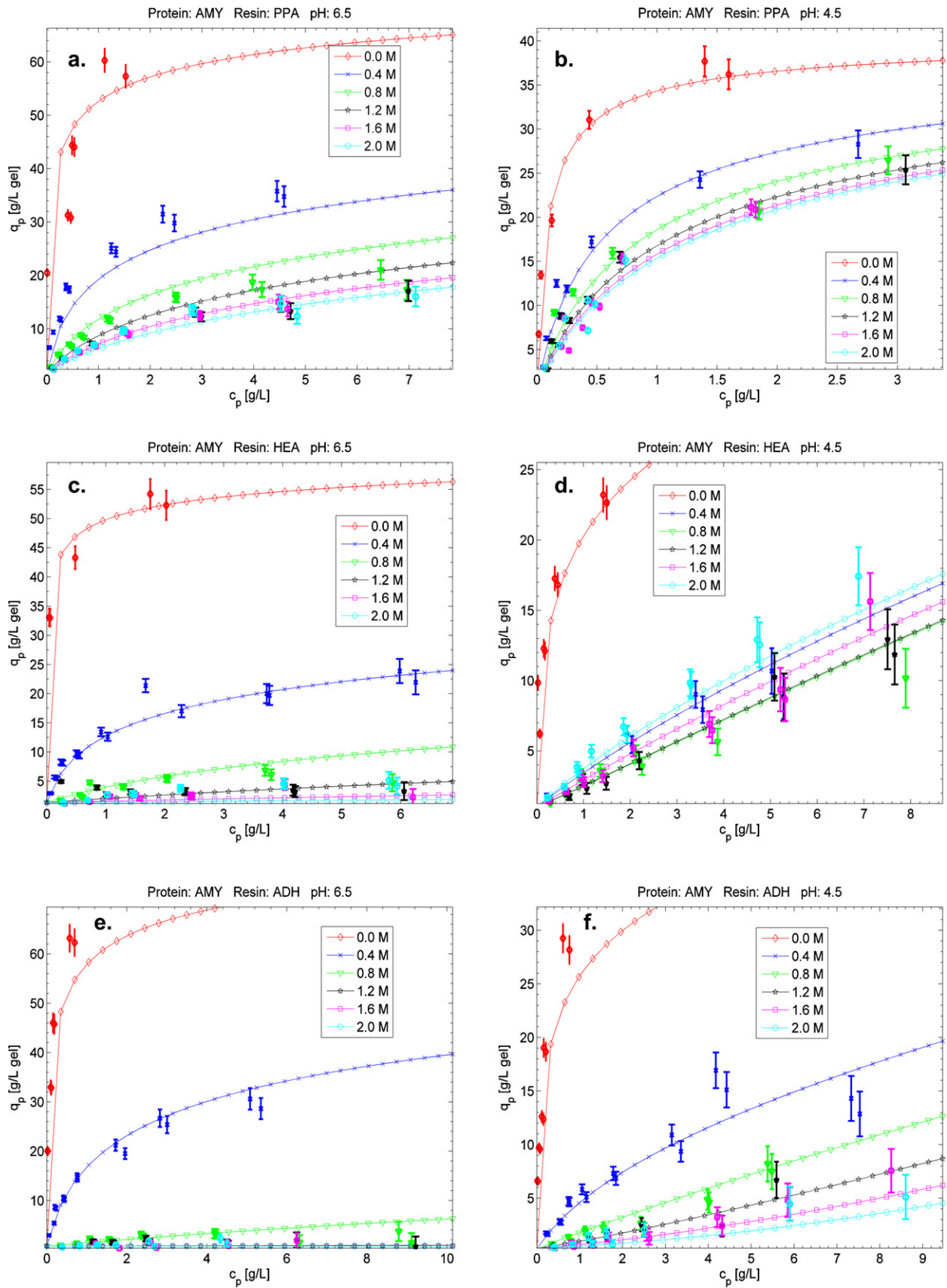
Fig. 10. Effects of NaCl salt concentration, pH and type of ligand on the adsorption isotherms of α-chymotrypsin (CHY) on PPA, HEA and ADH. (a) PPA, pH 9.0; (b) HEA, pH 9.0; (c) ADH, pH 9.0; (d) ADH, pH 6.5. Symbols with error bars represent experimental data and the solid lines represent fitted results from the mixed mode isotherm in Eq. (13). The different NaCl concentrations are given by the colour legends. (For interpretation of the references to colour in this figure legend, the reader is referred to the web version of the article.)
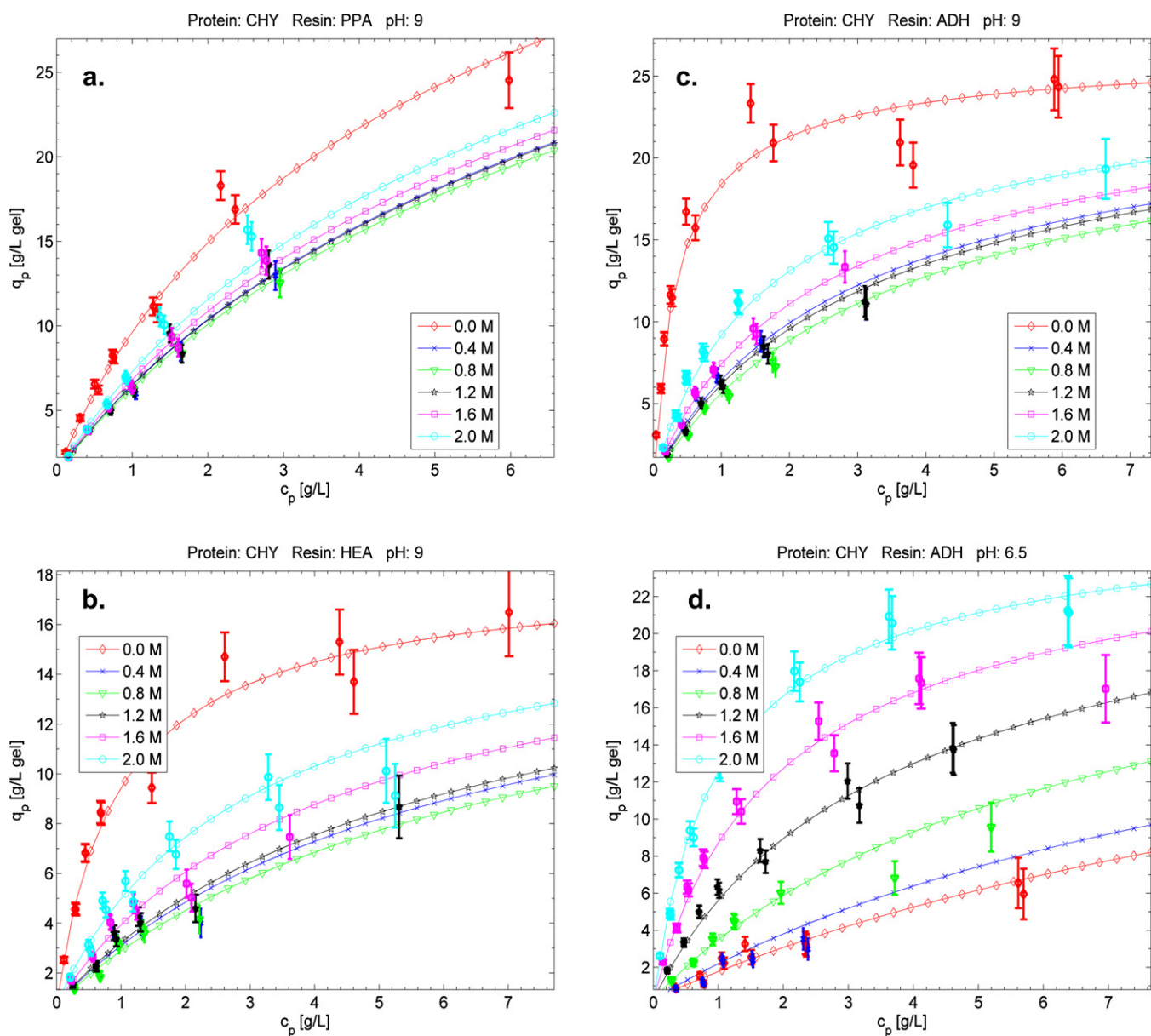
then a non-zero threshold salt concentration ($c_{s,min} > 0$) exists. For $K_s < 0$, the calculated threshold salt concentration ($c_{s,min}$) is negative, which is physically meaningless. In other words, when K_s is negative, the minimum point can no longer be reliably predicted by the isotherm model.

To analyze the situation when the interaction parameter K_s is negative, let us consider for a moment the definition of the interaction parameters K_s and K_p in the activity coefficient model in Eq. (16) as derived by Mollerup from the van der Waals equation of state [17]. If we denote the aqueous solvent, protein and salt by subscripts 1, 2 and 3, respectively, then:

$$K_s = \frac{2}{RT}(a_{12} - a_{32}) \tag{23}$$

$$K_p = \frac{2}{RT}(a_{12} - a_{22}) \tag{24}$$

where R is the molar gas constant, T is the temperature, a_{12}, a_{22} and a_{32} are the water–protein, protein–protein and salt–protein interaction constants, respectively, and depend on the charge on the protein and thus on pH [17].

According to Eq. (23), $K_s > 0$ implies that water–protein interactions are stronger than salt–protein interactions, and the reverse is true for $K_s < 0$. When $K_s \approx 0$, both interactions are of equal strength. The same can be said of the water–protein and the protein–protein interactions based on the sign of K_p. Similarly, a comparison between salt–protein and protein–protein interactions can be undertaken by considering the difference between K_s and K_p. Hence, the relative strengths of water–protein, protein–protein and salt–protein interactions can be deduced by comparing the different interaction parameters.

According to the results presented in Table 4, it is obvious that K_p is always greater than or equal to zero, indicating that protein–protein interactions were either equal ($K_p \approx 0$) or weaker

Table 4
Fitted isotherm parameters of protein adsorption on mixed mode resins.

Resin–protein–pH	Ln (K_{eq})	z_p	n	K_p (mM^{-1})	K_s (M^{-1})	$q_{p,MM}^{max}$ (mg/mL gel)	$c_{s,min}$ (mM)
PPA-BSA-6.5	18 ± −13	0.392 ± 0.076	4.467 ± 0.049	140 ± 13	−0.66 ± 0.12	22.64 ± 0.59	–
PPA-BSA-5.5	17 ± −12	0.258 ± 0.090	4.453 ± 0.064	130 ± 14	−1.11 ± 0.19	19.83 ± 0.68	–
HEA-BSA-6.5	19 ± −17	1.73 ± 0.14	4.40 ± 0.11	9.0 ± 8.5	1.32 ± 0.15	34.3 ± 3.5	1316
HEA-BSA-4.5	16 ± −16	0.000 ± 0.075	5.036 ± 0.081	0 ± 20	0.69 ± 0.19	45 ± 20	0
ADH-BSA-6.5	19 ± −19	3.24 ± 0.15	5.999 ± 0.081	37.7 ± 3.3	−0.58 ± 0.45	53.8 ± 2.9	–
ADH-BSA-5.5	1.5 ± 2.4	0.380 ± 0.081	0.3 ± 1.1	0.0 ± 5.2	−1.55 ± 0.47	13 ± 12	–
ADH-BSA-4.5	16 ± −19	1.297 ± 0.061	7.913 ± 0.073	0.0 ± 2.3	5.16 ± 0.18	96.5 ± 6.7	252
MMC-BSA-6.5	2.5 ± 3.2	2.55 ± 0.21	0.99 ± 0.69	42.2 ± 5.6	2.88 ± 0.39	18.8 ± 2.2	885
MMC-BSA-5.5	18 ± −15	0.00 ± 0.13	3.96 ± 0.11	0 ± 14	−9.31 ± 0.77	17.5 ± 1.6	–
MMC-BSA-4.5	13.0 ± −6.9	0.19 ± 0.14	2.372 ± 0.092	69 ± 22	−1.09 ± 0.22	32.8 ± 1.3	–
PPA-LYS-9.0	6.2 ± −6.7	0.00 ± 0.34	1.14 ± 0.21	0.0 ± 2.8	0.71 ± 0.32	57 ± 11	0
PPA-LYS-6.5	7.1 ± −8.1	0.00 ± 0.44	1.90 ± 0.28	0.0 ± 2.3	1.25 ± 0.43	61 ± 14	0
HEA-LYS-9.0	11 ± −12	0.00 ± 0.36	3.52 ± 0.23	1.6 ± 1.6	1.65 ± 0.35	99 ± 16	0
HEA-LYS-6.5	12 ± −12	0.00 ± 0.43	4.24 ± 0.29	1.2 ± 1.1	1.90 ± 0.40	104 ± 20	0
ADH-LYS-9.0	−1.4 ± −2.6	0.00 ± 0.25	0.12 ± 0.28	0.93 ± 0.53	1.99 ± 0.20	33.5 ± 3.9	0
ADH-LYS-6.5	−1.3 ± −2.9	0.00 ± 0.22	0.05 ± 0.23	0.00 ± 0.33	1.73 ± 0.18	31.4 ± 2.5	0
MMC-LYS-9.0	10 ± −10	3.197 ± 0.084	0.000 ± 0.063	5.5 ± 2.0	0.89 ± 0.19	60.7 ± 6.2	3597
MMC-LYS-6.5	17 ± −15	6.33 ± 0.14	0.00 ± 0.12	24.2 ± 4.8	1.99 ± 0.31	51.6 ± 4.7	3185
PPA-OVA-6.5	19 ± −23	1.239 ± 0.062	4.753 ± 0.050	12.8 ± 4.2	0.82 ± 0.08	67.4 ± 5.6	1512
PPA-OVA-4.5	17 ± −17	0.000 ± 0.042	4.995 ± 0.034	1.1 ± 4.8	0.35 ± 0.08	129 ± 27	0
HEA-OVA-6.5	19 ± −21	1.791 ± 0.059	4.733 ± 0.046	0.7 ± 1.6	1.51 ± 0.07	83.1 ± 6.0	1187
HEA-OVA-4.5	12 ± −15	0.000 ± 0.059	3.818 ± 0.042	0.0 ± 2.3	1.02 ± 0.11	113 ± 22	0
ADH-OVA-6.5	15 ± −17	2.16 ± 0.14	5.012 ± 0.057	3.4 ± 5.4	0.66 ± 0.45	140 ± 18	3249
ADH-OVA-4.5	3.9 ± −5.4	0.000 ± 0.047	1.485 ± 0.045	0.0 ± 4.2	0.34 ± 0.08	26 ± 19	0
PPA-AMY-6.5	18 ± −16	2.03 ± 0.15	3.839 ± 0.088	0.0 ± 5.4	0.52 ± 0.21	97.0 ± 4.6	3926
PPA-AMY-4.5	7.5 ± −2.9	0.98 ± 0.12	0.542 ± 0.077	0 ± 25	0.38 ± 0.17	40.3 ± 7.0	2575
HEA-AMY-6.5	19 ± −16	3.04 ± 0.40	3.31 ± 0.18	0.0 ± 7.6	−0.89 ± 0.80	75 ± 10	–
HEA-AMY-4.5	18 ± −18	2.51 ± 0.19	4.971 ± 0.068	20.3 ± 7.6	2.47 ± 0.27	62.5 ± 8.7	1016
ADH-AMY-6.5	19 ± −19	0.20 ± 0.15	4.827 ± 0.084	0.0 ± 4.3	−9.47 ± 0.75	108.4 ± 9.4	–
ADH-AMY-4.5	19 ± −20	2.015 ± 0.090	6.282 ± 0.051	12.6 ± 5.4	−0.19 ± 0.31	79.9 ± 7.8	–
PPA-CHY-9.0	7.8 ± −8.5	0.341 ± 0.032	2.013 ± 0.019	0.0 ± 2.1	0.43 ± 0.05	73 ± 32	800
HEA-CHY-9.0	2.5 ± 3.0	1.156 ± 0.068	0.00 ± 0.60	0.0 ± 1.7	1.56 ± 0.11	17.8 ± 4.6	742
ADH-CHY-9.0	3.3 ± 3.2	1.302 ± 0.042	0.00 ± 0.36	0.0 ± 1.3	1.58 ± 0.07	26.5 ± 3.0	824
ADH-CHY-6.5	2.7 ± 2.8	0.198 ± 0.044	1.07 ± 0.47	0.0 ± 1.0	1.76 ± 0.08	27.2 ± 5.5	112

($K_p > 0$) than water–protein interactions, but never greater under the conditions examined. On the other hand, K_s was either greater than zero or negative, i.e. salt–protein interactions were important under the conditions investigated in this study.

The results in Table 4 show that $K_s < 0$ (i.e. salt–protein interactions are dominant) for BSA and AMY under certain conditions (i.e. PPA-BSA-6.5, PPA-BSA-5.5, ADH-BSA-6.5, ADH-BSA-5.5, MMC-BSA-5.5, MMC-BSA-4.5, HEA-AMY-6.5, ADH-AMY-6.5, and ADH-AMY-4.5). It is worthy of note that the protein adsorption data in these cases could only be fitted when the lower bound on K_s was allowed to be negative. The fitted isotherms are shown in Figs. 4a, 4b, 5a, 5b, 5e, 5f, 9e and 9f, respectively. The figures show that the protein binding capacity decreases with increasing salt concentration when $K_s < 0$, indicating the stronger influence of electrostatic interactions under such conditions compared to hydrophobic interactions.

Two classical theories can be used to explain the mechanism of electrostatic protein–ligand interactions in the absence and in the presence of salt–protein interactions. These are the stoichiometric displacement theory [31] and the counter-ion condensation theory [23,32], respectively. According to the stoichiometric displacement theory, physical interactions between the charged protein and the oppositely charged stationary phase are mandatory for electrostatic interactions to occur, and protein adsorption occurs by displacement of counter-ions (ion-exchange) on the ligand surface [31]. The counter-ion condensation theory, on the other hand, assumes that protein molecules are atmospherically interacting with a counter-ion condensation layer over the surface of the oppositely charged stationary phase and do not physically interact with the stationary phase, but are kept in its vicinity by the electrostatic field generated by the fixed charges on the surface of the stationary phase [32]. This theory was applied by Melander

et al. to describe electrostatic interactions in ion-exchange chromatography [23].

Since the theoretical framework used in this study is a modification of the stoichiometric displacement model, the obtained effective charge represents physical ion-exchange interactions. The presence of salt–protein interactions may promote electrostatic protein adsorption by another mechanism, such as the counter-ion condensation mechanism, not described by the model. It appears that the inability of the mixed mode isotherm to reliably predict the minimum protein binding point in the presence of salt–protein interactions is related to this shift in electrostatic interaction mechanism under those conditions. However, the model could still describe the protein adsorption isotherm data under those conditions very well because it incorporates the activity coefficients of the species. Since K_s in the employed activity coefficient model gives a measure of salt–protein interactions, it is also possible to determine which electrostatic interaction mechanism could be dominant in a given system. For example, if $z_p > 0$ and $K_s < 0$ (e.g. PPA-BSA-6.5, PPA-BSA-5.5, ADH-BSA-6.5, ADH-BSA-5.5, MMC-BSA-4.5, HEA-AMY-6.5, ADH-AMY-6.5 and ADH-AMY-4.5), it is likely that both mechanisms are present. If $z_p > 0$ and $K_s > 0$, then the ion-exchange electrostatic interaction mechanism is dominant. If $z_p \approx 0$ and $K_s < 0$ (e.g. MMC-BSA-5.5), then the counter-ion condensation electrostatic interaction mechanism dominates. In this case the protein actually has an effective interaction charge, but this cannot be determined by the model since physical interactions are almost absent. Finally, if $z_p \approx 0$ and $K_s > 0$, then electrostatic interactions are almost non-existent. To investigate why salt–protein interactions were prominent only with BSA and AMY, the molecular masses and titration curves of the model proteins used in this study were considered. The titration curves were calculated by summing up the charge contributions of all charged (acidic and basic) amino
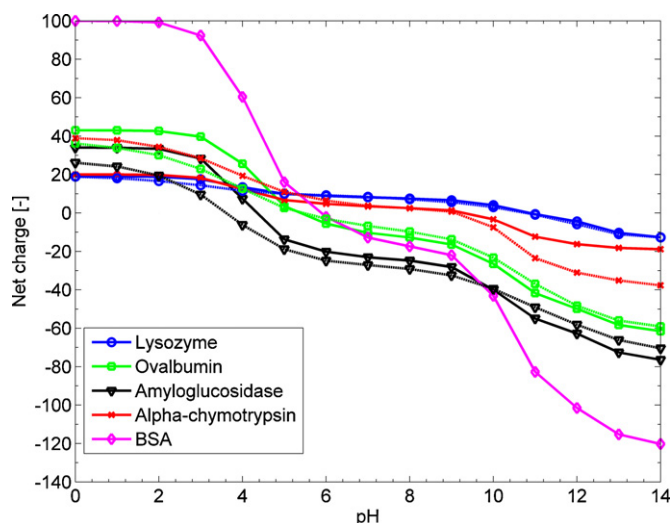
Fig. 11. Titration curves of model proteins calculated from the amino acid sequences (bold lines) as well as from their 3D structures (dotted lines). The 3D structure of BSA was not available in the RCSB Protein Data Bank (PDB) (http://www.rcsb.org/pdb).

acids and the C- and N-terminals as a function of the pH and the amino acid pK_as [33,34], Eq. (25):

$$z_{net} = \sum_i - \frac{N_{-i}}{1 + 10^{pK_{a_i}-pH}} + \sum_i \frac{N_{+i}}{1 + 10^{pH-pK_{a_i}}} \qquad (25)$$

where z_{net} is the protein net charge, N_- is the number of each acidic amino acid (Tyr, Cys, Asp, Glu) and the C-terminal, N_+ is the number of each basic amino acid (Lys, Arg, His) and the N-terminal. The first term on the right hand side of Eq. (25) gives the total negative charge contribution of all acidic amino acids and the C-terminal, while the second term gives the total positive charge contribution of all basic amino acids and the N-terminal.

The protein net charge was calculated by two different approaches. In the first approach, the net charge was calculated using pK_a values of the free amino acids and the amino acid sequence of each model protein was obtained from the ExPASy Proteomics Server (http://www.expasy.org). However, pK_a values of the free amino acids may differ significantly from those of the amino acid residues in the protein structure [35]. In the second approach, the actual amino acid pK_as, taking into account changes in the free amino acid pK_a due to interactions of the amino acid residue within the protein structure, were used instead of the free amino acid pK_as. These were estimated by making use of the 3D structures of the proteins obtained from the RCSB Protein Data Bank (PDB) (http://www.rcsb.org/pdb), and the method and computer program (PROPKA) developed by Jensen and co-workers [35,36]. In both approaches, Cys residues involved in disulfide bonds as well as ligands were excluded from the calculations. Slightly different pK_a values of the free amino acids are reported in the literature [35,37]. In this study, the free amino acid pK_a values from Jensen and co-workers [35] were used. All calculations were performed in MATLAB. The protein titration curves are shown in Fig. 11.

Although titration curves calculated from the 3D structures of proteins are generally more reliable, Fig. 11 shows that protein titration curves calculated using amino acid pK_a values obtained by the two different approaches do not differ significantly in the investigated pH range (pH 4.5–9.0). Hence, for BSA whose 3D structure was not available in the RCSB Protein Data Bank, the titration curve based on amino acid sequence was used instead.

It is also clear from Fig. 11 that the titration curves of BSA, OVA and AMY are much steeper than those of LYS and CHY below physiological pH. This means that a small change in pH would result in a

large change in their net charges under those conditions. Additionally, BSA and AMY are fairly large proteins compared to the others (see Table 2), with molecular masses of ∼66.4 kDa and ∼97 kDa, respectively. The large sizes of these proteins together with the steep nature of their titration curves may result in the protein surfaces becoming highly charged with even small shifts in pH, which may explain their propensity to interact with salts under some conditions (i.e. $K_s < 0$). pH shift typically occurs in the vicinity of a charged adsorbent surface due to the Donnan effect [3], and depends on the charge state of the adsorbent.

The fitted maximum protein binding capacities of the mixed mode adsorbents are summarized in Table 4. Obviously, under conditions where hydrophobic interactions are dominant (i.e. $z_p \approx 0$ and $K_s > 0$), the maximum protein binding capacity of the mixed mode adsorbent is mainly due to hydrophobic interactions, i.e. $q_{p,HIC}^{max} \approx q_{p,MM}^{max}$. Likewise, if conditions are chosen such that electrostatic interactions predominate (i.e. $n \approx 0$), then $q_{p,IEX}^{max} \approx q_{p,MM}^{max}$. If, however, the protein adsorption shows significant mixed mode behavior or salt tolerance, then the fitted saturation capacity is the net result of electrostatic and hydrophobic interactions.

Here, $q_{p,MM}^{max}$ is a salt independent quantity that gives the maximum protein saturation capacity of the mixed mode adsorbent, as oppose to the binding capacity in the traditional Langmuir isotherm that gives the apparent binding capacity at each salt concentration and so needs to be calculated for each salt concentration separately.

4.5. Influence of solution pH and salt concentration on protein adsorption isotherms

A systematic analysis of the influence of solution pH and salt concentration on the mixed mode protein adsorption isotherms obtained in this study is presented below by combining the quantitative information provided by the isotherm parameters and the qualitative information from the isotherm plots. Three different scenarios are considered: (1) the protein and ligand possess opposite global (net) surface charges; (2) the protein is neutrally charged; and (3) the protein and ligand are similarly charged. For each of these scenarios, the prevailing interaction mechanism is deduced from the effective charge (z_p), the number of hydrophobic ligands (n), the salt–protein interaction parameter (K_s) and the threshold salt concentration ($c_{s,min}$) as described earlier. The isotherms are discussed for each protein separately.

4.5.1. Adsorption isotherms of bovine serum albumin (BSA)

The iso-electric point (pI) of BSA is ∼5.5 [38,39]. BSA adsorption isotherms were determined at three different pH values; pH 4.5, 5.5 and 6.5. The adsorption isotherms of BSA on PPA and HEA are given in Fig. 4 and those on ADH and MMC are shown in Fig. 5.

BSA adsorption isotherms on PPA, HEA, ADH and MMC under conditions where the protein and ligand possess opposite net charges (i.e. at pH 6.5 for PPA, HEA and ADH, and pH 4.5 for MMC) are presented in Figs. 4a, 4c, 5a and 5f, respectively. The figures show that BSA binding capacity decreases with increasing salt concentration in all these cases, and, except for HEA-BSA-6.5, no salt-tolerance is observed under the conditions studied. Thus, it can be tempting to conclude that only electrostatic interactions are present. However, a close examination of the isotherm parameters in Table 4 shows that both z_p and n are non-zero in all the above cases, and so salt-tolerant protein adsorption should occur. This is, indeed, the case for HEA-BSA-6.5 where salt tolerance occurs at 1316 mM NaCl. However, no salt-tolerance is observed with PPA-BSA-6.5, ADH-BSA-6.5 and MMC-BSA-4.5, and although it is clear from the figures that the minimum protein binding occurs somewhere beyond the investigated salt concentration range (i.e. above

2 M NaCl), this point could not be reliably predicted due to the dominance of salt–protein interactions ($K_s < 0$).

BSA adsorption isotherms on PPA, ADH and MMC at pH 5.5 (pI of BSA) are presented in Figs. 4b, 5b and 5e, respectively. The isotherms show similar trends as in the previous scenario, i.e. BSA binding capacity decreases with increasing salt concentration, suggesting that electrostatic interactions are dominant. Since salt–protein interactions dominate ($K_s < 0$) also at pH 5.5, the same arguments as presented above for PPA-BSA-6.5, ADH-BSA-6.5 and MMC-BSA-4.5 hold. However, the protein should normally not possess a net charge or undergo electrostatic interactions at its pI, yet it does (PPA-BSA-5.5, ADH-BSA-5.5 and MMC-BSA-5.5).

There are two possible explanations why BSA still undergoes electrostatic interactions at pH 5.5 (pI of BSA). Firstly, the surface charge distribution on BSA could be heterogeneous, such that electrostatic interactions are still possible through patch-controlled protein adsorption, even if the protein does not possess a net surface charge. Secondly, the local pH in the micro-environment of the adsorbents could be different from that in the bulk solution, thereby promoting electrostatic interactions by the Donnan effect [3]. According to the Donnan effect, the formation of an electrical double layer around a charged adsorbent-liquid interface may attract negative ions and exclude protons (in the case of an anion-exchanger) thereby increasing the local pH around the adsorbent by up to 1 pH unit; or attract protons and exclude negative ions (in the case of a cation-exchanger) thereby decreasing the pH of the micro-environment by up to 1 pH unit [3]. This effect could be significant at solution pH close to the pI of the protein. That is, the change in the local pH around the ion-exchanger, combined with the steep nature of the BSA titration curve, could change the net surface charge of BSA molecules in the vicinity of the adsorbent sufficiently to promote electrostatic interactions.

BSA adsorption isotherms on HEA, ADH and MMC under conditions of electrostatic charge repulsion (HEA-BSA-4.5, ADH-BSA-4.5 and MMC-BSA-6.5) are presented in Figs. 4d, 5c and 5d, respectively. Only HEA-BSA-4.5 shows the expected behavior. That is, $z_p \approx 0$ and the hydrophobic binding mode is dominant, with protein binding capacity increasing with increasing salt concentration and minimum protein binding occurs at 0 M NaCl. Here, the surface hydrophobicity of the protein is the main driving force for protein adsorption. On the other hand, electrostatic BSA interactions occur on ADH and MMC even under electrostatic repulsion conditions (pH 4.5 for ADH and pH 6.5 for MMC). Since n and K_s are also greater than zero in both cases, salt-tolerant protein adsorption behavior was expected. This was, indeed, observed, with a minimum point at 252 mM NaCl for ADH-BSA-4.5 and at 885 mM NaCl for MMC-BSA-6.5 (Figs. 5c and d, respectively). The presence of electrostatic interactions under electrostatic repulsion conditions can be attributed to the heterogeneity of surface charge distribution on BSA that leads to the patch-controlled protein adsorption mechanism described earlier [8,15,30]. Infact, salt-tolerant BSA adsorption on mixed mode adsorbents under electrostatic charge repulsion conditions has been described by other researchers [8,14,15,25].

Furthermore, BSA adsorption on MMC shows a transition from favorable to unfavorable binding above 0 M NaCl under charge repulsion conditions (Fig. 5d). This has been observed before for BSA on Streamline Direct HST mixed mode adsorbent that bears the same functional group as MMC [8]. The authors proposed the multi-layer BSA adsorption mechanism to explain this phenomenon. In the multi-layer BSA adsorption mechanism, first a single layer of BSA molecule is adsorbed via the patch-controlled mechanism. Then a second layer of BSA molecules can be formed through protein–protein electrostatic interactions between BSA molecules in solution and the adsorbed BSA at dimer docking sites

[8]. In this way, the adsorbed protein layer may grow unfavorably (linearly or exponentially) with increasing liquid phase protein concentration.

The influence of solution pH on the maximum binding capacity of BSA on the different mixed mode adsorbents is shown in Fig. 13a. In all cases, the minimum protein binding occurred at pH 5.5. For MMC, the maximum binding capacity of BSA occurs at pH 4.5. This is in agreement with the literature, where the maximum BSA binding capacity on STREAMLINE Direct HST having the same ligand as MMC was found between pH 4 and 5 [8,24]. For HEA and ADH, the maximum BSA binding capacity was equally observed at pH 4.5. ADH shows the highest binding capacity for BSA within the specified standard errors.

4.5.2. Adsorption isotherms of lysozyme (LYS)

Lysozyme has a pI of ~11. Adsorption isotherms of LYS were measured at pH 6.5 and pH 9, where LYS possesses a net positive charge (pH < pI). The adsorption isotherms of LYS on PPA and HEA are shown in Fig. 6 and those on ADH and MMC are shown in Fig. 7.

Isotherms of LYS on PPA, HEA and ADH (Figs. 6a–d, 7a and 7b) are all obtained under charge repulsion conditions (pH 6.5 and pH 9) where the protein and ligand possess a net positive charge. Under these conditions, $z_p \approx 0$ and the hydrophobic interaction mode is expected to dominate the protein adsorption. This is, indeed, the case as evidenced by the increasing hydrophobic binding with increasing salt concentration and a $c_{s,min}$ at 0 M NaCl. In these cases, protein elution can simply be achieved at low salt concentration where there is almost no protein binding. It must be stressed, however, that in the presence of electrostatic interactions under charge repulsion conditions like in the case of BSA, much harsher elution conditions (e.g. drastic pH changes) are needed to effect protein elution.

LYS adsorption isotherms under conditions favorable for electrostatic charge interactions are those on MMC at pH 9 (Fig. 7c) and MMC at pH 6.5 (Fig. 7d). MMC has a weak cation exchange group with a pK_a ~3 and so is negatively charged at those pH values. Salt-tolerant protein adsorption is observed in both cases, with $c_{s,min}$ at 3597 mM NaCl and 3185 mM NaCl for LYS on MMC at pH 9 and pH 6.5, respectively.

The influence of solution pH on the maximum binding capacity of LYS on the different mixed mode adsorbents is shown in Fig. 13b. For PPA and HEA, LYS binding capacities are about the same at pH 6.5 and at pH 9 within the specified standard errors. This is probably due to the flat nature of the titration curve of LYS between pH 6.5 and 9 (see Fig. 11), which indicates that the net charge on LYS (pI ~11) only slightly changes within this pH range and likewise the strengths of electrostatic charge repulsion at pH 6.5 and 9. Although PPA and HEA (pK_a ~8) may lose some fraction of their positive charges at pH > pK_a (e.g. at pH 9), thereby weakening electrostatic charge repulsions compared to at pH 6.5, the results show that this effect is probably quite minimal at pH 9. Likewise, no appreciable change in LYS binding capacity with pH is observed for ADH and MMC in going from pH 6.5 to pH 9. HEA performs best under the investigated conditions. ADH, on the other hand shows the lowest LYS binding capacity (Fig. 13b).

4.5.3. Adsorption isotherms of ovalbumin (OVA)

Ovalbumin has a pI of ~4.9. Adsorption isotherms of OVA were measured at pH 4.5 and at pH 6.5 and for the anion-exchange mixed mode resins (PPA, HEA and ADH) only. The adsorption isotherms of OVA on PPA, HEA and ADH are shown in Fig. 8.

Isotherms of OVA on PPA, HEA and ADH at pH 6.5 where the protein and ligand are oppositely charged are shown in Fig. 8a, c and e, respectively. As expected, electrostatic interactions are prominent at pH 6.5 and OVA shows salt-tolerant adsorption with minimum point at 1512 mM NaCl, 1187 mM NaCl and 3249 mM on PPA, HEA
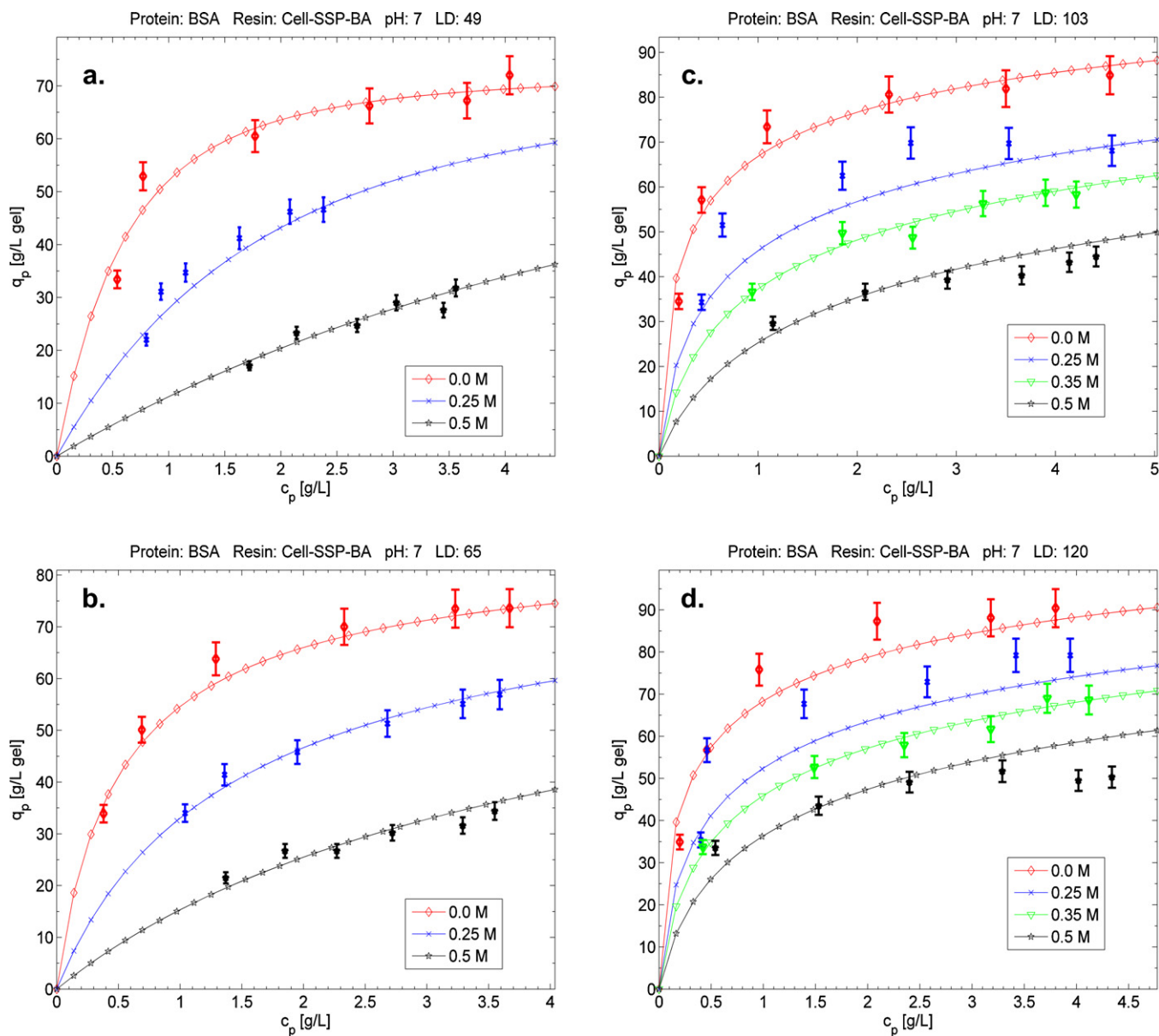
Fig. 12. Effects of NaCl salt concentration and ligand density on the adsorption isotherms of BSA on Cell-SSP-BA at pH 7.0. (a) Cell-SSP-BA-4, ligand density (LD) = 49 mmol/L gel; (b) Cell-SSP-BA-3, ligand density (LD) = 65 mmol/L gel; (c) Cell-SSP-BA-2, ligand density (LD) = 103 mmol/L gel; (d) Cell-SSP-BA-1, ligand density (LD) = 120 mmol/L gel. Symbols with error bars represent experimental data from Gao et al. [14] and the solid lines represent fitted results from the mixed mode isotherm in Eq. (13). The different NaCl concentrations are given by the colour legends. (For interpretation of the references to colour in this figure legend, the reader is referred to the web version of the article.)

and ADH, respectively. Like for MMC-LYS-9.0 and MMC-LYS-6.5 (Fig. 7c and d, respectively), the salt tolerance on ADH-OVA-6.5 (Fig. 8e) occurs outside the investigated salt concentration range of 0–2 M NaCl. Hence, one would have been tempted to conclude the absence of salt tolerance in these cases if only a qualitative analysis was undertaken. The occurrence of salt tolerance can also explain the low sensitivity to changes in salt concentration (isotherms are closer together) at high salt concentrations (typically above 0.4 M NaCl). The same can be said of BSA adsorption on HEA at pH 6.5.

Adsorption isotherms of OVA on PPA, HEA and ADH under charge repulsion conditions are depicted in Fig. 8b, d and f, respectively. Here too, the expected trend is observed, with protein binding strength increasing with increasing salt concentration due to hydrophobic interactions and minimum protein adsorption occurs at 0 M NaCl, in accordance with the theory ($z_p \approx 0$, $n > 0$

and $c_{s,min} \approx 0$). Appreciable protein adsorption is observed even at 0 M NaCl. Since electrostatic interactions are minimal ($z_p \approx 0$ and $K_s > 0$), this can be attributed to the hydrophobic nature of OVA at pH 4.5 (close to its pI), strong enough to overcome the electrostatic repulsive forces at that pH.

The influence of solution pH on the maximum binding capacity of OVA on the different mixed mode adsorbents is shown in Fig. 13c. Higher OVA binding capacities were obtained for PPA and HEA at pH 4.5 than at pH 6.5. This can be attributed to a switch from the more dominant IEX mode at pH 6.5 to the more dominant HIC mode at pH 4.5 (Fig. 8). Hence, except for ADH, the strength of hydrophobic OVA interactions at pH 4.5 surpasses that of electrostatic charge repulsion at the same pH. The much lower binding capacity of OVA on ADH at pH 4.5 compared to those on PPA and HEA is probably due to stronger electrostatic repulsions on ADH which has a strong anion-exchange group.
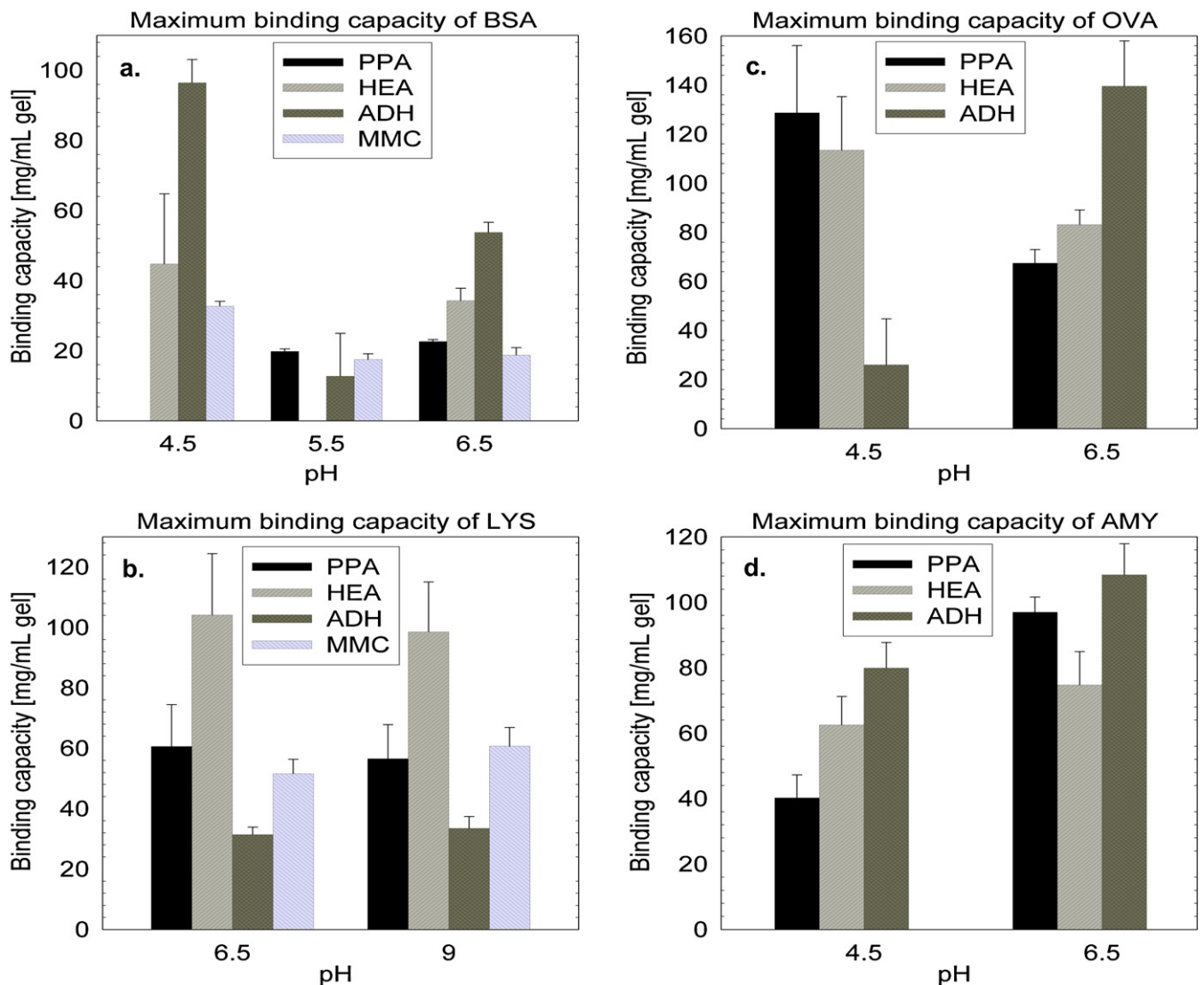
Fig. 13. Effect of pH on protein binding capacities on mixed mode resins. (a) Bovine serum albumin (BSA); (b) lysozyme (LYS); (c) ovalbumin (OVA); (d) amyloglucosidase (AMY). The different mixed mode resins are given by the legends.

4.5.4. Adsorption isotherms of amyloglucosidase (AMY)

Amyloglucosidase has a pI of ~3.9. Adsorption isotherms were obtained for AMY at pH 4.5 and at pH 6.5 and for the anion-exchange mixed mode resins (PPA, HEA and ADH) only. The adsorption isotherms of AMY on PPA, HEA and ADH are shown in Fig. 9.

At the investigated pH values (4.5 and 6.5), AMY is oppositely charged with respect to PPA, HEA and ADH. Except for ADH, AMY possesses a higher effective binding charge at pH 6.5 than at pH 4.5 as expected (Table 4). AMY shows the expected salt-tolerant adsorption on PPA at both pH conditions and on HEA at pH 4.5, with minimum protein binding occurring at 3926 mM, 2575 mM, and 1016 mM for PPA-AMY-6.5, PPA-AMY-4.5, and HEA-AMY-4.5, respectively. However, this minimum point occurs above 2 M NaCl for PPA and so is not obvious on the isotherms (Fig. 9a and b). Salt tolerance is clearly visible for HEA-AMY-4.5 (Fig. 9d). Low sensitivity to changes in salt concentration can also be observed above 0.4 M NaCl due to this salt-tolerant behavior. Salt-tolerant AMY adsorption was, however, not observed on ADH at both pH values and on HEA at pH 6.5 due to stronger salt–protein interactions ($K_s < 0$) that changes the electrostatic interaction mechanism in favor of the counter-ion condensation mechanism. Hence, the minimum point could not be reliably predicted in these cases, although

it certainly occurred at much higher salt concentrations than those investigated. The higher effective binding charge of AMY on ADH at pH 4.5 could be due to heterogeneous charge distribution on the surface of the protein.

The influence of solution pH on the maximum binding capacity of AMY on the different mixed mode adsorbents is shown in Fig. 13d. AMY has higher binding capacities at pH 6.5 than at pH 4.5. The binding capacity on ADH is higher than those on PPA and HEA under the conditions examined. This could be due to the reinforcement of AMY adsorption on ADH by hydrogen bonding as well as by the presence of salt–protein interactions.

4.5.5. Adsorption isotherms of α-chymotrypsin (CHY)

The pI of α-chymotrypsin is ~8.7. Isotherms of CHY were determined at pH 9 on PPA, HEA and ADH (Fig. 10a–c), and at pH 6.5 on ADH (Fig. 10d). At pH 9, CHY is oppositely charged with respect to the mixed mode ligands (PPA, HEA and ADH). As expected, salt tolerant CHY adsorption is observed, with minimum binding at 800 mM, 742 mM and 824 mM NaCl for PPA-CHY-9.0, HEA-CHY-9.0 and ADH-CHY-9.0, respectively. The salt tolerance brings about the observed low sensitivity to salt concentration above 0 M NaCl.

At pH 6.5, CHY experiences charge repulsions on ADH. The results show that CHY still possesses an effective binding charge and shows salt tolerant binding on ADH even at pH 6.5. Salt tolerance occurs at 112 mM NaCl, although that is not obvious on the isotherm because this condition was not investigated (Fig. 10d). It appears that when salt tolerance occurs at low salt concentration (e.g. ADH-BSA-4.5 and ADH-CHY-6.5), the sensitivity of the protein binding capacity to changes in salt concentration is less affected than when it happens at high salt concentration (e.g. PPA-CHY-9.0, HEA-CHY-9.0, and ADH-CHY-9.0).

4.6. Influence of ligand chemistry on mixed mode protein adsorption

The type and density of mixed mode ligand also have important consequences for mixed mode protein adsorption.

4.6.1. Influence of ligand type

A fair comparison of the influence of the type of mixed mode ligand on protein adsorption is difficult, given that the ligands possess different electrostatic and hydrophobic groups, except for PPA and HEA which bear the same charge group (amine group) and differ only in their hydrophobic groups (a phenylpropyl group for PPA and a hexyl group for HEA). Both resins also have similar average ligand densities (see Table 1).

In general, PPA and HEA show comparable protein binding capacities with BSA, OVA and AMY within the presented standard errors, but the actual outcome depends on the specific resin–protein–pH combination. For example, PPA shows a slightly better OVA binding capacity than HEA at pH 4.5 and a lower one at pH 6.5. On the other hand, PPA shows a lower AMY binding capacity than HEA at pH 4.5 and a higher one at pH 6.5. Furthermore, HEA shows much higher LYS binding capacity than PPA at pH 6.5 and 9, although the latter is more hydrophobic and both resins have the same electrostatic functional group (i.e. they both experience similar electrostatic charge repulsion at a given pH). This could be attributed to the slightly higher ligand density and hence better accessibility of the hexylamine group on HEA compared to the phenylpropylamine group on PPA. Compared to PPA, ADH generally shows better binding capacities under conditions more favorable for electrostatic interactions (e.g. BSA, OVA and AMY at pH 6.5 in Fig. 13a, c and d). Since PPA and ADH both have the phenyl hydrophobic group, this differences in binding capacities can be attributed to the strong nature of the anion-exchange group on ADH and the fact that it bears hydrogen bonding groups close to its electrostatic group that assist protein binding under favorable electrostatic conditions. For the same reasons, ADH also shows stronger electrostatic repulsions under electrostatic charge repulsion conditions and hence lower binding capacities than PPA and HEA (e.g. OVA at pH 4.5, LYS at pH 6.5 and 9.0 in Fig. 13), except where electrostatic interacts still play a significant role (e.g. BSA and AMY at pH 4.5).

4.6.2. Influence of ligand density

The influence of ligand density on mixed mode protein adsorption was studied by considering BSA adsorption isotherm data on four Cell-SSP-BA mixed mode adsorbents having the same benzylamine functional group but with different ligand densities (49, 65, 103 and 120 mmol/L gel), obtained from Gao et al. [14]. The protein binding capacity of these adsorbents increased with increasing ligand density, but more stringent elution conditions were required [14]. A trade-off between binding capacity and the required elution conditions is therefore required when choosing the appropriate ligand density for mixed mode adsorbents.

As shown in Fig. 12, the BSA adsorption data on Cell-SSP-BA from Gao et al. [14] could be successfully fitted with the mixed mode

isotherm formalism in Eq. (13). Hence, the mixed mode isotherm formalism presented in this study can be used with any mixed mode adsorbent having the hydrophobic and electrostatic functional groups.

5. Conclusions

The thermodynamic modeling of protein adsorption on mixed-mode adsorbents functionalized with ligands carrying both hydrophobic and electrostatic groups was undertaken. The developed mixed mode isotherm was fitted with protein adsorption data obtained for five different proteins (BSA, lysozyme, ovalbumin, amyloglocusidase and α-chymotrypsin) on four different mixed mode adsorbents from two different suppliers (PPA HyperCel and HEA HyperCel from PALL Life Sciences, Capto Adhere and Capto MMC from GE HealthCare) by 96-well microtitre plate high throughput batch experiments on a robotic workstation.

The influence of salt concentration on the protein adsorption was explicitly incorporated and the mixed mode isotherm could describe measured protein adsorption data at different salt concentrations very well. The effective protein charge was found to be strongly pH-dependent and generally decreased towards the pI of the protein, but was not a function of salt concentration. The protein binding capacity, on the other hand, was a strong function of both the salt concentration and the solution pH. No correlation was found between the solution pH and the number of hydrophobic ligands nor the equilibrium constant.

The isotherm parameters enabled a more quantitative analysis of the observed isotherm behaviors. For example, where the number of interacting hydrophobic ligands, $n \approx 0$, electrostatic interactions were predominant and the protein binding capacity decreased with increasing salt concentration. On the other hand, where the effective protein binding charge, $z_p \approx 0$, the hydrophobic interaction mode was predominant for $K_S > 0$, and the protein binding capacity increased with increasing salt concentration. Mixed mode protein adsorption showed salt-tolerant behavior for z_p and n greater than zero, taking into account the standard errors on these parameters.

The threshold salt concentration at which minimum protein adsorption occurs could be precisely determined from the slope of the mixed mode isotherm as a function of salt concentration to be v/K_S, where v is the ion-exchange stoichiometric coefficient ($v = z_p/z_s$) and K_S is the salt–protein interaction parameter. A $K_S < 0$ implies that salt–protein interactions are stronger than water–protein interactions, and vice versa. For $K_S > 0$, calculated values of the threshold salt concentrations were in excellent agreement with the protein adsorption isotherms. However, when salt–protein interactions were dominant (i.e. $K_S < 0$) the minimum protein binding could no longer be reliably predicted by the isotherm model. This was thought to be due to a possible transition in the prevalent electrostatic interaction mechanism from the classical counter-ion exchange mechanism to the counter-ion condensation mechanism or other salt-mediated electrostatic interaction mechanism not captured by the model.

Salt–protein interactions were dominant only for BSA and amyloglucosidase. The propensity of BSA and amyloglucosidase to undergo salt–protein interacts was attributed to a combination of factors including the large size of the proteins, the steep nature of their titration curves, as well as the charge state of the mixed mode adsorbent.

The occurrence of electrostatic protein–ligand interactions ($z_p > 0$ or $K_S < 0$) under unfavorable pH conditions was equally observed in some cases. For example, PPA-BSA-5.5, ADH-BSA-5.5, MMC-BSA-5.5, ADH-BSA-4.5, MMC-BSA-6.5 and ADH-CHY-6.5. This could be due to the heterogeneous charge distribution on the surface of the proteins which promotes patch-controlled protein

adsorption, and/or the Donnan effect which causes pH shifts around the microenvironment of the adsorbent. Unfavorable BSA adsorption was observed on MMC at pH 6.5 in the presence of salt.

When salt-tolerant protein adsorption occurred, the sensitivity of the protein binding capacity to changes in salt concentration decreased as the turning point or threshold salt concentration was approached. That is, when the threshold salt concentration was high, the isotherms were closer to each other at high salt concentration, and when it was low, the isotherms were further apart. Of all the isotherms that showed salt-tolerant behavior, only those of BSA on ADH at pH 4.5 and of α-chymotrypsin on ADH at pH 6.5 fall in the latter category (Table 4 and Figs. 4–10).

The influence of mixed mode ligand chemistry on the protein adsorption was equally studied. PPA and HEA generally showed comparable protein binding capacities, except for LYS, where HEA was clearly better. ADH generally showed better binding capacities than PPA and HEA under conditions more favorable for electrostatic interactions (e.g. OVA and AMY at pH 6.5 in Fig. 13c and d), but also stronger electrostatic repulsions and lower binding capacities than PPA and HEA under electrostatic charge repulsion conditions (e.g. OVA at pH 4.5, LYS at pH 6.5 and 9.0 in Fig. 13). These could be attributed to the strong nature of the anion-exchange group on ADH and the fact that it bears hydrogen bonding groups close to its electrostatic group.

The developed mixed mode isotherm was capable of describing the adsorption isotherms of all five proteins (having widely different molecular masses and iso-electric points) on the four mixed mode adsorbents and over a wide range of salt concentrations and solution pH, and provided a unique set of physically meaningful parameters for each resin–protein–pH combination. The possibility of predicting the salt concentration at which minimum protein binding occurs presents new opportunities for designing better elution strategies in mixed mode protein chromatography. Finally, the mixed mode isotherm also gave very good fit with literature data of BSA adsorption on another mixed mode adsorbent functionalized with benzylamine ligands. Hence, the mixed mode isotherm formalism presented in this study can be used with any mixed mode adsorbent having the hydrophobic and electrostatic functional groups. It also provides the basis for detailed modeling and optimization of mixed mode chromatographic separation of proteins.

Nomenclature

a	activity
a	interaction parameter
A	initial slope of isotherm or partition coefficient
c	molar concentration of solution in the pore volume
c_L	molar concentration of free ligands
c_p	molar concentration of protein in the liquid phase
c_s	molar concentration of salt
q_p	molar concentration of protein in the adsorbed phase
G°	standard Gibbs energy of association
K_{eq}	equilibrium constant
K_s	difference between water–protein and salt–protein interactions
K_p	difference between water–protein and protein–protein interactions
M_r	molecular mass
n	stoichiometric coefficient of hydrophobic ligand
R	molar gas constant
T	temperature
v	stoichiometric coefficient of salt counter-ion
V	volume
z_p	effective protein charge
z_s	charge on salt counter-ion

Greek letters

γ	activity coefficient
$\tilde{\gamma}$	asymmetric activity coefficient
Λ	ligand density
σ	steric hindrance factor in IEX
δ	steric hindrance factor in HIC
Δ	difference between G° in the adsorbed state and the solute state

Subscripts

12	water–protein
22	protein–protein
32	salt–protein
eq	equilibrium
exp	experimental
H	liquid hold-up
HIC	hydrophobic interaction chromatography
IEX	ion-exchange chromatography
MM	mixed mode
i	component i
j	component j
k	data point k
$load$	dispensed liquid
L	ligand
p	protein
PL_n	protein–ligand complex
sim	simulated
s	salt
SL	salt–ligand complex
W	water

Superscripts

max	maximum
∞,w	at infinite dilution in water

Acknowledgements

References

[1] B.K. Nfor, P.D.E.M. Verhaert, L.A.M. van der Wielen, J. Hubbuch, M. Ottens, Trends Biotechnol. 27 (2009) 673.
[2] B.K. Nfor, T. Ahamed, G.v. Dedem, L.A.M.v.d. Wielen, E.J.A.X.v.d. Sandt, M. Eppink, M. Ottens, J. Chem. Technol. Biotechnol. 83 (2008) 124.
[3] R.K. Scopes, Protein Purification: Principles and Practice, Springer-Verlag, New York, Inc., 1994.
[4] D. Gao, S.-J. Yao, D.-Q. Lin, J. Appl. Polym. Sci. 107 (2008) 674.
[5] L.A. Kennedy, W. Kopaciewicz, F.E. Regnier, J. Chromatogr. 359 (1986) 73.
[6] G. Zhao, X.-Y. Dong, Y. Sun, J. Biotechnol. 144 (2009) 3.
[7] V. Brenac Brochier, A. Schapman, P. Santambien, L. Britsch, J. Chromatogr. A 1177 (2008) 226.
[8] D. Gao, D.-Q. Lin, S.-J. Yao, J. Chromatogr. B 859 (2007) 16.
[9] S. Ghose, B. Hubbard, S.M. Cramer, Biotechnol. Prog. 21 (2005) 498.
[10] M.L. Heinitz, L. Kennedy, W. Kopaciewicz, F.E. Regnier, J. Chromatogr. 443 (1988) 173.
[11] G.E. Hamilton, F. Luechau, S.C. Burton, A. Lyddiatt, J. Biotechnol. 79 (2000) 103.
[12] K.A. Kaleas, C.H. Schmelzer, S.A. Pizarro, J. Chromatogr. A 1217 (2010) 235.
[13] Y. Shi, R. Xiang, C. Horváth, J.A. Wilkins, J. Chromatogr. A 1053 (2004) 27.
[14] D. Gao, D.-Q. Lin, S.-J. Yao, J. Chem. Eng. Data 51 (2006) 1205.
[15] D. Gao, D.-Q. Lin, S.-J. Yao, Biochem. Eng. J. 38 (2008) 355.
[16] C.A. Brooks, S.M. Cramer, AIChE J. 38 (1992) 1969.
[17] J.M. Mollerup, Fluid Phase Equilibr. 241 (2006) 205.
[18] J.M. Mollerup, Chem. Eng. Technol. 31 (2008) 864.
[19] S. Yamamoto, Chem. Eng. Technol. 28 (2005) 1387.
[20] J.M. Mollerup, T.B. Hansen, S. Kidal, A. Staby, J. Chromatogr. A 1177 (2008) 200.

[21] R.W. Deitcher, J.E. Rome, P.A. Gildea, J.P. O'Connell, E.J. Fernandez, J. Chromatogr. A 1217 (2010) 199.
[22] J.M. Mollerup, T.B. Hansen, S. Kidal, L. Sejergaard, A. Staby, Fluid Phase Equilibr. 261 (2007) 133.
[23] W.R. Melander, Z. El Rassi, C. Horváth, J. Chromatogr. 469 (1989) 3.
[24] Y.-K. Chang, S.-Y. Chou, J.-L. Liu, J.-C. Tasi, Biochem. Eng. J. 35 (2007) 56.
[25] P. Li, G. Xiu, V.G. Mata, C.A. Grande, A.E. Rodrigues, Biotechnol. Bioeng. 94 (2006) 1155.
[26] J.L. Coffman, J.F. Kramarczyk, B.D. Kelley, Biotechnol. Bioeng. 100 (2008) 605.
[27] T. Bergander, K. Nilsson-Välimaa, K. Öberg, K.M. Lacki, Biotechnol. Prog. 24 (2008) 632.
[28] D.W. Marquardt, SIAM J. Appl. Math. 11 (1963) 431.
[29] Evaluation of Measurement Data—Guide to the Expression of Uncertainty in Measurement, Joint Committee for Guides in Metrology (JCGM), http://www.bipm.org/en/committees/jc/jcgm/wg1.html, 2008.

[30] V. Lesins, E. Ruckenstein, Colloid Polym. Sci. 266 (1988) 1187.
[31] W. Kopaciewicz, M.A. Rounds, J. Fausnaugh, F.E. Regnier, J. Chromatogr. 266 (1983) 3.
[32] G.S. Manning, Q. Rev. Biophys. 11 (1978) 179.
[33] J.M. Ribeiro, A. Sillero, Comput. Biol. Med. 20 (1990) 235.
[34] J.M. Ribeiro, A. Sillero, Comput. Biol. Med. 21 (1991) 131.
[35] L. Hui, D.R. Andrew, H.J. Jan, Proteins: Struct. Funct. Bioinform. 61 (2005) 704.
[36] D.C. Bas, D.M. Rogers, J.H. Jensen, Proteins: Struct. Funct. Bioinform. 73 (2008) 765.
[37] A. Sillero, A. Maldonado, Comput. Biol. Med. 36 (2006) 157.
[38] W.W.P. Chang, C. Hobson, D.C. Bomberger, L.V. Schneider, Electrophoresis 26 (2005) 2179.
[39] T. Ahamed, B.K. Nfor, P.D.E.M. Verhaert, G.W.K. van Dedem, L.A.M. van der Wielen, M.H.M. Eppink, E.J.A.X. van de Sandt, M. Ottens, J. Chromatogr. A 1164 (2007) 181.